

Reduced plakoglobin increases the risk of sodium current defects and atrial conduction abnormalities in response to androgenic anabolic steroid abuse

Sommerfeld, Laura C.; Holmes, Andrew P.; Yu, Ting Y.; O'Shea, Christopher; Kavanagh, Deirdre M.; Pike, Jeremy M.; Wright, Thomas; Syeda, Fahima; Aljehani, Areej; Kew, Tania; Cardoso, Victor R.; Kabir, S. Nashitha; Hepburn, Claire; Menon, Priyanka R.; Broadway-Stringer, Sophie; O'Reilly, Molly; Witten, Anika; Fortmueller, Lisa; Lutz, Susanne; Kulle, Alexandra

DOI:

[10.1113/jp284597](https://doi.org/10.1113/jp284597)

License:

Creative Commons: Attribution (CC BY)

Document Version

Publisher's PDF, also known as Version of record

Citation for published version (Harvard):

Sommerfeld, LC, Holmes, AP, Yu, TY, O'Shea, C, Kavanagh, DM, Pike, JM, Wright, T, Syeda, F, Aljehani, A, Kew, T, Cardoso, VR, Kabir, SN, Hepburn, C, Menon, PR, Broadway-Stringer, S, O'Reilly, M, Witten, A, Fortmueller, L, Lutz, S, Kulle, A, Gkoutos, GV, Pavlovic, D, Arlt, W, Lavery, GG, Steeds, R, Gehmlich, K, Stoll, M, Kirchhof, P & Fabritz, L 2024, 'Reduced plakoglobin increases the risk of sodium current defects and atrial conduction abnormalities in response to androgenic anabolic steroid abuse', *The Journal of Physiology*.
<https://doi.org/10.1113/jp284597>

[Link to publication on Research at Birmingham portal](#)

General rights

Unless a licence is specified above, all rights (including copyright and moral rights) in this document are retained by the authors and/or the copyright holders. The express permission of the copyright holder must be obtained for any use of this material other than for purposes permitted by law.

- Users may freely distribute the URL that is used to identify this publication.
- Users may download and/or print one copy of the publication from the University of Birmingham research portal for the purpose of private study or non-commercial research.
- User may use extracts from the document in line with the concept of 'fair dealing' under the Copyright, Designs and Patents Act 1988 (?)
- Users may not further distribute the material nor use it for the purposes of commercial gain.

Where a licence is displayed above, please note the terms and conditions of the licence govern your use of this document.

When citing, please reference the published version.














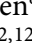
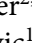




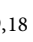
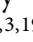
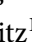




Take down policy

While the University of Birmingham exercises care and attention in making items available there are rare occasions when an item has been uploaded in error or has been deemed to be commercially or otherwise sensitive.

If you believe that this is the case for this document, please contact UBIRA@lists.bham.ac.uk providing details and we will remove access to the work immediately and investigate.

Download date: 12. May. 2024

Reduced plakoglobin increases the risk of sodium current defects and atrial conduction abnormalities in response to androgenic anabolic steroid abuse

Laura C. Sommerfeld^{1,2,3} , Andrew P. Holmes^{1,4} , Ting Y. Yu^{1,5}, Christopher O'Shea^{1,5} , Deirdre M. Kavanagh^{1,6} , Jeremy M. Pike^{1,6} , Thomas Wright¹, Fahima Syeda¹ , Areej Aljehani¹ , Tania Kew¹, Victor R. Cardoso^{1,7} , S. Nashitha Kabir¹ , Claire Hepburn¹ , Priyanka R. Menon¹ , Sophie Broadway-Stringer¹ , Molly O'Reilly¹ , Anika Witten^{8,9} , Lisa Fortmueller^{2,3,8} , Susanne Lutz¹⁰ , Alexandra Kulle¹¹ , Georgios V. Gkoutos^{2,12,7,13} , Davor Pavlovic¹ , Wiebke Arlt^{14,15,16} , Gareth G. Lavery^{14,15} , Richard Steeds^{1,17} , Katja Gehmlich¹ , Monika Stoll^{8,9,18} , Paulus Kirchhof^{1,3,19}  and Larissa Fabritz^{1,2,3,17,19} 

¹Institute of Cardiovascular Sciences, University of Birmingham, Birmingham, UK

²University Center of Cardiovascular Science, University Heart and Vascular Center, UKE Hamburg, Hamburg, Germany

³German Center for Cardiovascular Research (DZHK), Standort Hamburg/Kiel/Lübeck, Germany

⁴School of Biomedical Sciences, Institute of Clinical Sciences, University of Birmingham, Birmingham, UK

⁵Research and Training Centre in Physical Sciences for Health, Birmingham, UK

⁶Centre of Membrane Proteins and Receptors (COMPARE), University of Birmingham, Birmingham, UK

⁷Institute of Cancer and Genomic Sciences, University of Birmingham, Birmingham, UK

⁸Genetic Epidemiology, Institute for Human Genetics, University of Münster, Münster, Germany

⁹Core Facility Genomics of the Medical Faculty, University of Münster, Münster, Germany

¹⁰Institute of Pharmacology and Toxicology, University Medical Center Göttingen, Göttingen, Germany

¹¹Division of Paediatric Endocrinology and Diabetes, University Hospital Schleswig-Holstein, Campus Kiel, Kiel, Germany

¹²Institute of Translational Medicine, University Hospitals Birmingham NHS Foundation Trust, Birmingham, UK

¹³MRC Health Data Research UK (HDR), Midlands Site, UK

¹⁴Institute of Metabolism and Systems Research (IMSR), University of Birmingham, Birmingham, UK

¹⁵Centre for Endocrinology, Diabetes and Metabolism (CEDAM), Birmingham Health Partners, Birmingham, UK

¹⁶Medical Research Council London Institute of Medical Sciences, London UK & Institute of Clinical Sciences, Faculty of Medicine, Imperial College, London, UK

¹⁷Department of Cardiology, University Hospitals Birmingham NHS Foundation Trust, Birmingham, UK

¹⁸Cardiovascular Research Institute Maastricht, Department of Biochemistry, Maastricht University, Maastricht, The Netherlands

¹⁹Department of Cardiology, University Heart & Vascular Center Hamburg, University Medical Center Hamburg-Eppendorf, Hamburg, Germany

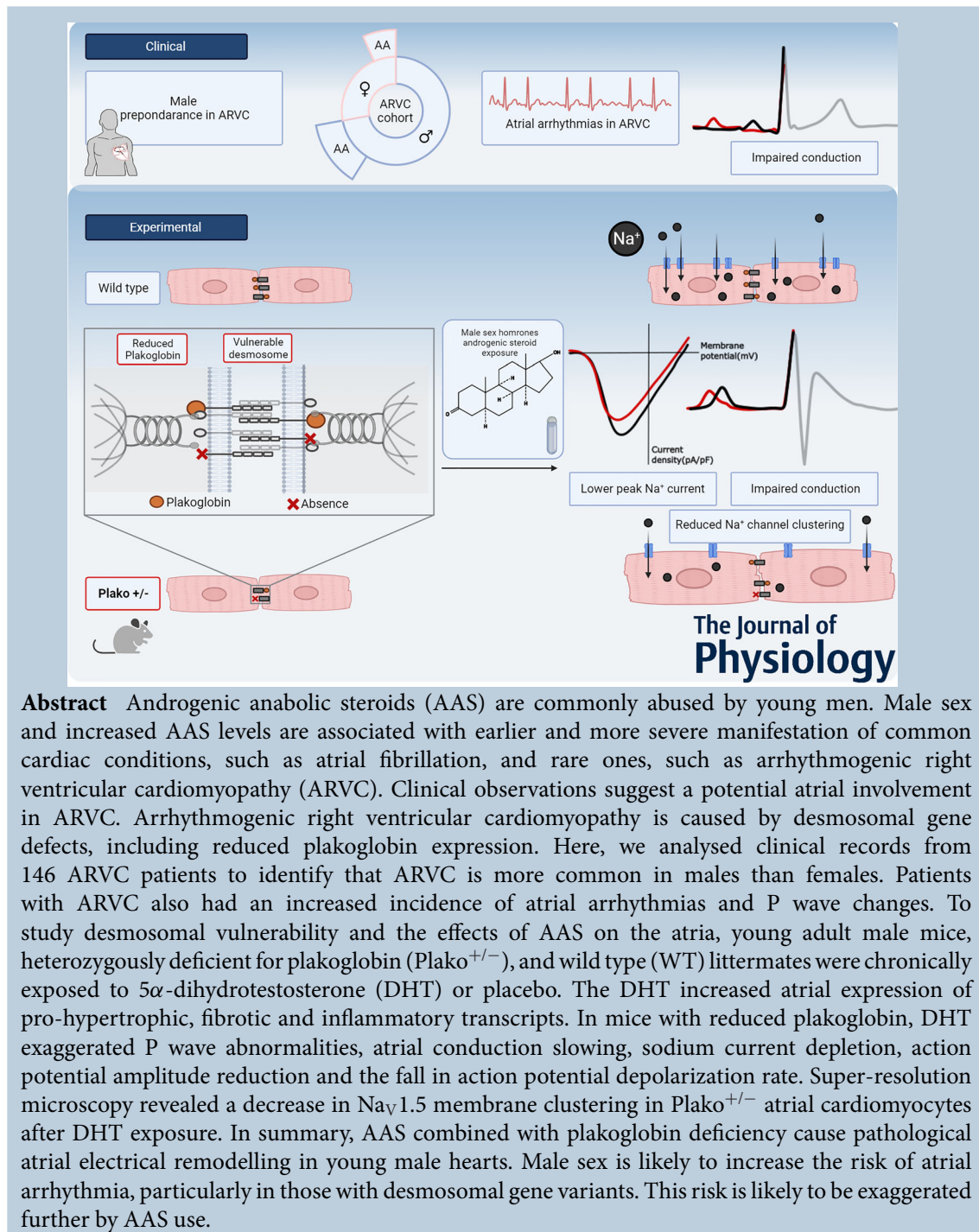
Handling Editors: Peter Kohl & Ramona Emig

The peer review history is available in the Supporting Information section of this article (<https://doi.org/10.1113/JP284597#support-information-section>).

Laura C. Sommerfeld, holding a BSc in Molecular Medicine, an MSc in Cardiovascular Sciences from University of Göttingen, Germany, and a PhD in Cardiovascular Sciences from University of Birmingham, UK, immersed herself in cardiac research across various institutions, such as the University Medical Centre Göttingen, University Medical Centre Hamburg-Eppendorf and King's College London. Her PhD thesis at Birmingham, UK, focused on 'deciphering inheritable drivers of atrial arrhythmia'. Currently a Postdoctoral Researcher at University Centre of Cardiovascular Science (UCCS) Hamburg, she enjoys working at the clinical and basic research interface and delves into molecular mechanisms of arrhythmias and cardiomyopathies, exploring desmosomal instability and atrial fibrillation biomarkers.



This article was first published as a preprint. Sommerfeld LC, Holmes AP, Yu TY, O'Shea C, Kavanagh DM, Pike JM, Wright T, Syeda F, Aljehani A, Kew T, Cardoso VR, Kabir SN, Hepburn C, Menon PM, Broadway-Stringer S, O'Reilly M, Witten A, Fortmueller L, Lutz S, Kulle A, Gkoutos GV, Pavlovic D, Arlt W, Lavery GG, Steeds R, Gehmlich K, Stoll M, Kirchhof P, Fabritz L. 2022. Male sex hormone and reduced plakoglobin jointly impair atrial conduction and cardiac sodium currents. bioRxiv. <https://doi.org/10.1101/2022.06.03.494748>



(Received 28 February 2023; accepted after revision 16 January 2024; first published online 10 February 2024)

Corresponding author L. Fabritz: University Centre of Cardiovascular Science, University Heart and Vascular Centre, UKE Hamburg, 20246 Hamburg, Germany. Email: l.fabritz@uke.de

Abstract figure legend Atrial arrhythmias (AA) can be a clinical manifestation of advanced arrhythmogenic right ventricular cardiomyopathy (ARVC), and a male preponderance can be observed. Patients with ARVC show atrial conduction abnormalities on ECG. In a murine experimental ARVC model, low expression of the ARVC-associated protein plakoglobin (Plako^{+/-}) combined with androgenic anabolic steroid (male sex hormone) exposure led to ECG

P wave abnormalities. This was combined with reduced sodium channel (Na_v1.5) clustering and decreased peak Na⁺ current, leading to atrial conduction abnormalities, a substrate for arrhythmias.

Key points

- Androgenic male sex hormones, such as testosterone, might increase the risk of atrial fibrillation in patients with arrhythmogenic right ventricular cardiomyopathy (ARVC), which is often caused by desmosomal gene defects (e.g. reduced plakoglobin expression).
- In this study, we observed a significantly higher proportion of males who had ARVC compared with females, and atrial arrhythmias and P wave changes represented a common observation in advanced ARVC stages.
- In mice with reduced plakoglobin expression, chronic administration of 5 α -dihydrotestosterone led to P wave abnormalities, atrial conduction slowing, sodium current depletion and a decrease in membrane-localized Na_v1.5 clusters.
- 5 α -Dihydrotestosterone, therefore, represents a stimulus aggravating the pro-arrhythmic phenotype in carriers of desmosomal mutations and can affect atrial electrical function.

Introduction

Several inherited arrhythmia syndromes develop more severe phenotypes in men carrying pathogenic variants, e.g. Brugada syndrome or arrhythmogenic right ventricular cardiomyopathy (ARVC) (Marcus et al., 2010). Male sex is also associated with a higher incidence of atrial arrhythmias, both in the general population and in rare conditions (Baturova et al., 2020; Camm et al., 2013; Chu et al., 2010; Morita et al., 2002; Priori et al., 2015; Tonet et al., 1991). Effects mediated by anabolic androgenic steroids (AAS), such as testosterone and the most potent androgen, 5 α -dihydrotestosterone (DHT), could contribute. Abuse of AAS is an emerging global health concern, not restricted to elite athletes but common in the general population, with reports indicating a 3.3% lifetime prevalence worldwide (Sagoe et al., 2014). AAS are abused predominately by men to increase muscle mass, improve athletic performance and alter appearance (Sagoe et al., 2014). However, AAS can cause cardiac pathology, including hypertrophy and electrophysiological changes (Alizade et al., 2015; Fineschi et al., 2007; Luijkx et al., 2013; Marsh et al., 1998; Medei et al., 2010; Pirompol et al., 2016; Urhausen et al., 2004). Atrial arrhythmias have recently been associated with elevated total plasma testosterone levels in men (Berger et al., 2019) and were observed in patients known to take AAS devoid of a clinical indication (Lau et al., 2007; Sullivan et al., 1999; Tsai et al., 2014). Despite these observations, the mechanisms underpinning atrial electrical remodelling in response to higher levels of AAS are largely unknown.

ARVC is often caused by variants in desmosomal genes, including plakoglobin (Antoniades et al., 2006; Asimaki et al., 2007; McKoy et al., 2000; Protonotarios et al., 2001), and has recently been reported to show more adverse

outcomes in men (Rootwelt-Norberg et al., 2021) related to sex hormone levels (Akdis et al., 2017).

We set out to investigate atrial changes in ARVC because there are associations of common gene variants close to desmosomal genes with atrial fibrillation (AF) (Roselli et al., 2018). We hypothesized that a substantial proportion of ARVC patients is suffering from clinically relevant atrial arrhythmias and that vulnerability of the desmosome, caused by, for example, plakoglobin reduction, might increase the risk of male sex hormone-induced atrial electrical remodelling.

To test this hypothesis, we screened patient records for atrial arrhythmias from definite and non-definite ARVC patients seen at a tertiary centre Inherited Cardiac Conditions Clinic. Furthermore, we used a murine ARVC model to study the effects of chronically elevated AAS levels in male mice with heterozygous plakoglobin (gamma-catenin) deficiency (Plako^{+/-}), an established animal model of ARVC (Kirchhof et al., 2006), and their wild type (WT) littermates.

Methods

Arrhythmogenic right ventricular cardiomyopathy patient record screening for atrial arrhythmias and semi-automated analysis of digital ECGs from ARVC patients

Adult ARVC patients (>18 years of age) seen at a specialty clinic at a tertiary centre between 2010 and 2021 (Aljehani et al., 2023) were classified into two disease severity groups, i.e. non-definite and definite cases, based on 2010 ARVC Task Force Criteria (TFC) (Marcus et al., 2010).

Clinical records were reviewed retrospectively to obtain information from several modalities, including imaging,

electrophysiology, histopathology, genetic testing and family history, to fulfil a diagnostic classification cumulatively. Patients exhibiting signs of confirmed disease based on specific combinations of minor or major criteria were classified as the 'definite' group. Individuals exhibiting signs on diagnostic investigation congruous with the 2010 TFC as 'borderline' or 'possible' ARVC were considered cumulatively as the 'non-definite' group because they do not confer a confirmed diagnosis of ARVC. Non-definite cases were included in the analysis to represent individuals in the earlier phases of disease with a less severe profile of phenotypic expression. As expected, right ventricular outflow tract diameter was increased, and tricuspid annular plane systolic excursion was lower (<20 mm) in patients with definitive ARVC, reflecting TFC. Left ventricular function was preserved in both groups. About one-third of the definite patients had engaged in competitive sports, whereas only every 10th patient of the non-definite group had a history of competitive sports. Following good clinical practice in the UK, genetic analysis was performed only if clinically indicated. Variants were found mostly in desmosomal genes (*PKP2*, plakophilin-2; *DSC2*, desmocollin-2; and *DSG2*, desmoglein-2). Atrial fibrillation and flutter status were extracted from previous ECGs and clinical letters.

Digital ECG recordings (10 s, sampling frequency 500 Hz) from the most recent follow-up in the Inherited Cardiac Conditions Clinic were collated and analysed using MATLAB (MathWorks, USA) and BioSigKit (<https://doi.org/10.21105/joss.00671>). To discern the extent of atrial involvement in definite ARVC patients in comparison to non-definite patients and control subjects, family members of index patients who did not meet task force diagnostic criteria or had ARVC pathogenic variants excluded from targeted gene panel testing were additionally included ('Control'). Digital ECG analysis was performed by multiple independent observers in recordings displaying sinus rhythm by applying a custom-designed, semi-automated algorithm. ECGs were digitally filtered between 0.5 and 50 Hz, and using a Chebyshev type II filter. The R wave was automatically identified, and all complexes within the recording were averaged to improve signal quality. The isoelectric line was defined from start to end of the P wave (Fig 1).

Animal husbandry

All animal procedures were approved by the UK Home Office (PPL number 30/2967 and PFDAAF77F) and by the institutional review board of the University of Birmingham. All animal procedures conformed to the guidelines from Directive 2010/63/EU of the European Parliament on the protection of animals used for scientific purposes. Wild type (WT) and plakoglobin-deficient

(Plako^{+/-}) male 129/Sv mice (Kirchhof et al., 2006) were housed in individually ventilated cages (two to seven mice per cage), in standard conditions: 12 h–12 h light–dark cycle, 22°C and 55% humidity. Food and water were available *ad libitum*. The general health status of all mice (bearing, grooming and behaviour) used in the study was monitored daily and immediately before all animal procedures.

Chronic 5 α -dihydrotestosterone exposure in the murine model and experimental timeline

Young adult male mice (8–11 weeks old) were assigned to either DHT or placebo/control treatment groups in mixed cages and were fitted with subcutaneous osmotic mini-pumps (Alzet 2006, USA; reservoir volume 0.2 ml), containing either DHT (62.5 mg/ml in ethanol) or solvent alone [Control (Ctr)], for 6 weeks (Fig. 2). Age and DHT exposure time were matched for all groups. Mice of comparable weight and ≥ 20 g were selected for pump implantation. Weight at pump implantation was 24 ± 0.5 g. At least 40 min before pump implantation, mice were injected s.c. with 0.05 ml of buprenorphine (National Veterinary Services, UK) for analgesia. Pump implantation was performed under general anaesthesia with isoflurane inhalation (maximum of 4%) in O₂, with a flow rate of 1–2 L/min. Animal handling staff and investigators were blinded to genotype and treatment. Echocardiography was performed at 6 weeks of exposure. Murine hearts were then extracted by thoracotomy under deep terminal anaesthesia [4–5% isoflurane (National Veterinary Services, UK) in O₂, flow rate 1–2 L/min], resulting in death by exsanguination. Extracted hearts were used immediately for *in organ* and *in vitro* experimental analysis, as summarized in Fig. 2.

Anabolic androgenic steroid measurements

Serum DHT was determined by ultra-performance liquid chromatography–tandem mass spectrometry (LC-MS/MS), as described by Kulle et al. (2010). In brief, aliquots of samples, calibrator and controls were combined with the internal standard mixture to monitor recovery. All samples were extracted using Oasis MAX SPE system Plates (Waters, USA). The chromatographic separation was carried out using an ultra-performance liquid chromatography (UPLC) system, which is connected to a Quattro Premier/XE triple Quad mass spectrometer (Waters, USA). A Waters Acquity UPLC BEH C18 column (1.7 μ m, 100 mm \times 2.1 mm) was used at a flow rate of 0.4 ml/min at 50°C. Water and acetonitril with 0.01% formic acid were used as the mobile phase. Two mass transitions were monitored. The following optimized voltages were used: capillary

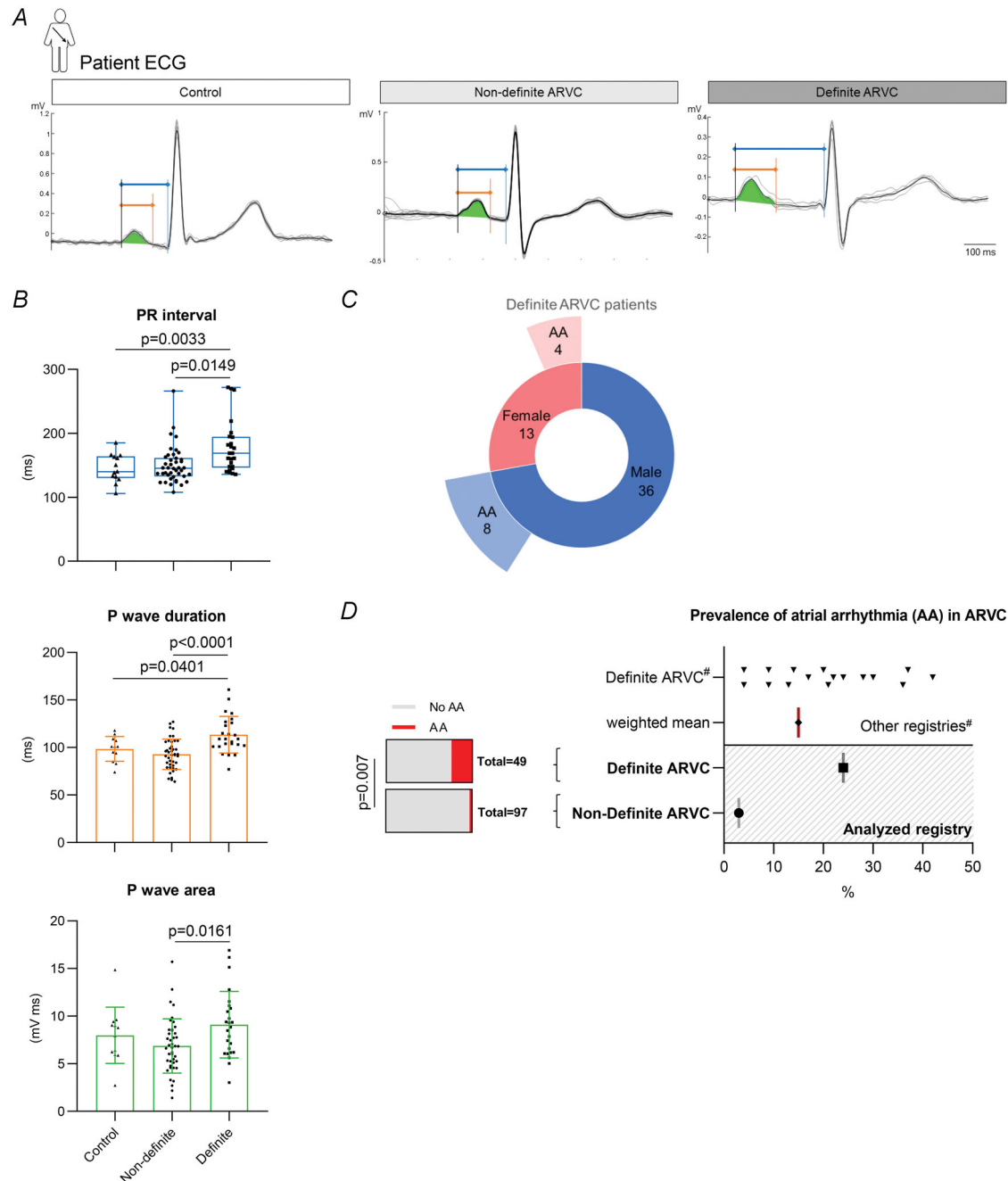


Figure 1. Atrial arrhythmias and P wave characteristics in arrhythmogenic right ventricular cardiomyopathy patients and control individuals

A, lead II ECG recordings from an unaffected individual (control) and a non-definite and definite ARVC patient. Individual cardiac cycles over a duration of 10 s (grey traces) are overlaid by detected R waves and averaged (black trace). The PR interval (blue), P wave duration (orange) and P wave area (green) are marked. B, PR interval (box plots with medians indicated) and P wave characteristics (means \pm SD indicated) obtained from semi-automated analysis of the averaged ECG. Heart rate (mean \pm SEM): control, 73 ± 3 beats/min; non-definite ARVC, 75 ± 2 beats/min; definite ARVC, 60 ± 3 beats/min. *P*-values from *post hoc* tests are reported on the graphs [Kruskal–Wallis ($P < 0.05$) with Dunn's *post hoc* test for PR interval; one-way ANOVA ($P < 0.05$) with Bonferroni *post hoc* test for P wave duration and area]. *n* (number of patients): control, 12; non-definite ARVC, 42; definite ARVC, 25. C, sex distribution and prevalence of AA in definite ARVC patients in the analysed registry. D, prevalence of AA in definite ARVC patients in other registries (with weighted mean indicated) and in definite and non-definite ARVC patients in the registry analyzed here. #Please refer to Table 3 for detailed references. Abbreviations: AA, atrial arrhythmia; ARVC, arrhythmogenic right ventricular cardiomyopathy.

voltage 3.5 kV, cone voltage 28–33 V; collision energy 18–25 eV; dwell time 0.01–0.08 s depending on the steroid; source temperature 120°C; and desolvation temperature 450°C. Argon was used as the collision gas. Data were acquired with MassLynx v.4.1 software, and quantification was performed by TargetLynx software (Waters, USA). During all analyses, the ambient temperature was kept at 21°C by air conditioning. Analyses had the following parameters: limit of detection 0.054 nmol/L; limit of quantification 0.1 nmol/L; inter-assay coefficient of

variation 4–8% for 0.75 and 7.5 nmol/L; and intra-assay between 2 and 3%.

Murine ECG measurements

Murine surface six-lead ECGs were recorded from mice using a tunnel system (ecgTunnel, EMKA Technologies, France), with contact electrodes installed in the tunnel floor. The ECG recording started after a short adaptation period. All measurements were conducted during

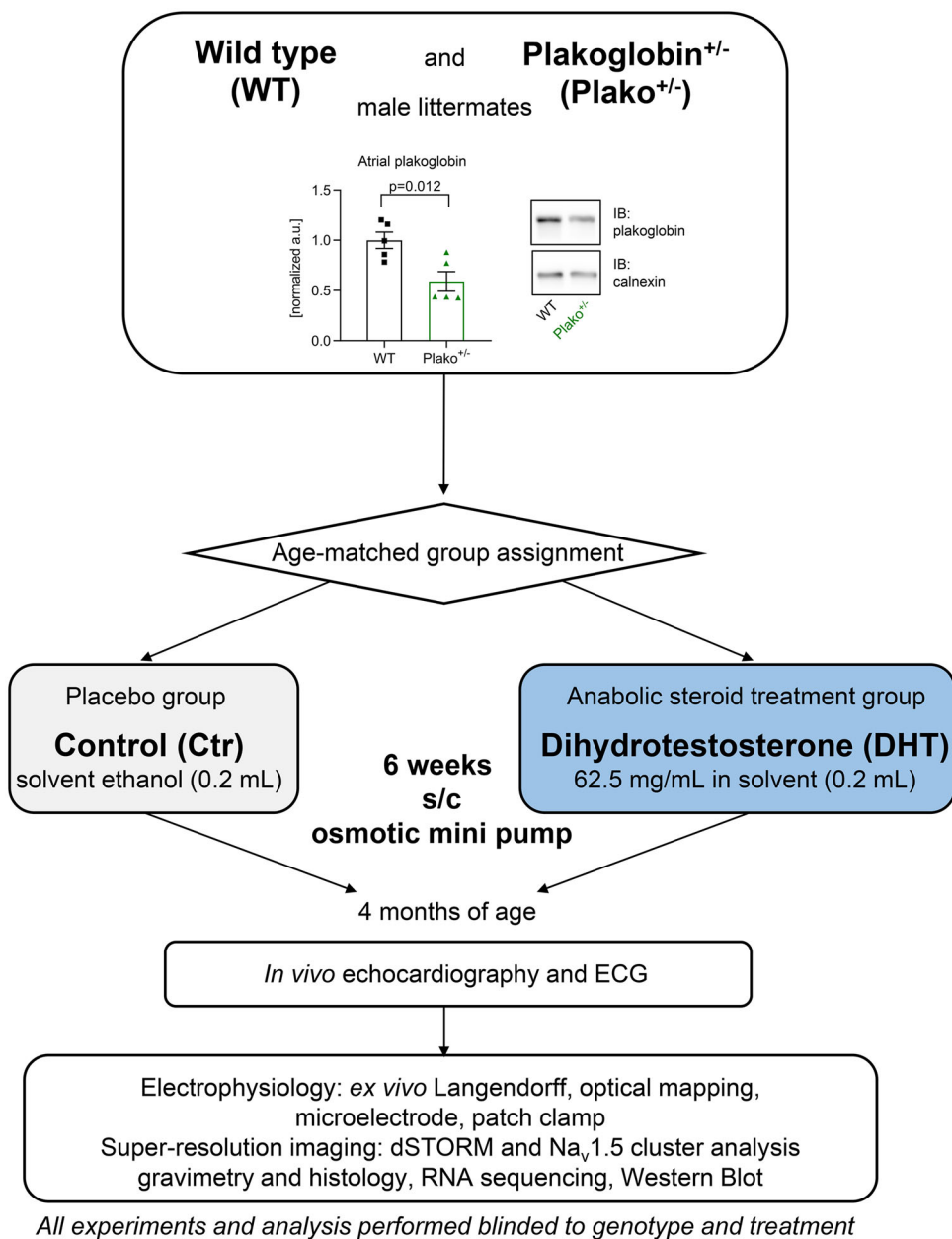


Figure 2. Genetic model and study design for murine experiments

Experimental time-line and methods used in the murine study. Top, atrial plakoglobin expression normalized to calnexin and representative immunoblots (IB); $n = 5$ atria per group. All results described were obtained in male wild type (WT) or Plako^{+/-} mice at 4 months of age after exposure to either 5 α -dihydrotestosterone (DHT) or placebo control (Ctr) for 6 weeks.

daytime. Mean ECG recording time was ~ 4 min (3.64 ± 0.13 min) using the software IOX (EMKA Technologies, France).

The analysis of ECG recordings was performed blinded to genotype and group (placebo or DHT). All parameters were measured from lead II. Mean heart rate was measured by using the software ecgAUTO (EMKA Technologies, France). Heart beats detected by the software were checked for ECG quality, and ECG recordings were also scanned manually for arrhythmias and abnormalities by an experienced blinded observer. For better direct comparison, sections of similar heart rate (aiming for 645 beats/min) were selected.

The software was used to create averaged signals of 20 single beats delivering very clear ECG waves. Signals were chosen for similar P wave morphology and heart rate (to exclude heart rate-dependent effects). Three such summary averaged signals for each animal were analysed manually for P wave duration and for PR, QRS and QT intervals, and values obtained were averaged per animal.

Ex vivo beating murine heart Langendorff electrophysiological study

Electrograms from beating murine hearts were recorded in a previously reported Langendorff set-up (Obergassel et al., 2021). In brief, hearts were extracted, and the aorta was retrogradely perfused with Krebs–Henseleit (KH) solution at a coronary flow rate of 4 ml/min at 37°C. Hearts were left for 5 min to stabilize a base-line and then paced via the right atrium using an octapolar catheter (NUMED, USA), allowing for tracking of atrioventricular conduction. After determining the diastolic pacing threshold, S1 pacing was performed at twice threshold voltage, applying different cycle lengths of 120, 100 and 80 ms for 1 min each. Analysis of the occurrence of atrioventricular block was conducted in the ecgAUTO software environment (EMKA Technologies, France).

Optical mapping of murine left atria

Murine hearts were mounted on a vertical Langendorff apparatus (Hugo Sachs, Germany), and the aorta was retrogradely perfused at 36–37°C, pH 7.4 with KH solution plus Di-4-ANEPPS (17.5 μ M; potential-sensitive ANEP dye D1199, Cambridge Bioscience, UK). The left atrium (LA) was removed and pinned out in a recording chamber with the superior surface exposed (Holmes et al., 2016; Yu et al., 2014). The LA was continuously superfused with a KH solution containing (mM): NaCl, 118; NaHCO₃, 24.88; KH₂PO₄, 1.18; glucose, 5.55; MgSO₄, 0.83; CaCl₂, 1.8; and KCl, 3.52, equilibrated with 95% O₂–5% CO₂, pH 7.4. Blebbistatin (10 μ M; Cayman

Chemical, USA) was added to the superfusate to prevent contraction artefacts. After 15 min of equilibration, the LA was paced (pulses 2 ms in duration, two times diastolic voltage threshold) at 120–80 ms cycle length (CL) using bipolar platinum electrodes and a constant-voltage stimulator (Digitimer, UK). Di-4-ANEPPS was excited at 530 nm by four LEDs (Cairn Research, UK), and fluorescence was captured at 630 ± 20 nm using a second-generation, high-spatial-resolution CMOS ORCA flash 4.0 camera (Hamamatsu Photonics, Japan). Images were captured at a sampling rate of 0.987 kHz (128×2048 pixels) and digitized using WinFluor v.3.4.9 (Dr John Dempster, University of Strathclyde, UK).

Raw images were used to measure LA unfolded area manually in FIJI. Activation maps, conduction velocity vectors and optical action potentials were generated using MATLAB algorithms as described previously (Holmes et al., 2016; O'Shea et al., 2019; Syeda et al., 2016; Yu et al., 2014). Individual beat activation times were calculated from activation maps constructed by measuring the depolarization midpoint (time of 50% upstroke amplitude) of the optical action potential at each pixel. The percentage of tissue activation was then measured as a function of time, with time to 95% activation compared between the individual beats. To analyse conduction changes in more detail, beat-to-beat variability in whole tissue activation times was evaluated during rapid physiological pacing. To do this, 10 individual activation maps were compared from the final 10 beats of a train of 50 pulses at 80 ms CL.

Murine echocardiography

Echocardiography was performed as previously described at a target heart rate of 390–440 beats/min (Fabritz et al., 2011; Kirchhof et al., 2011) with a dedicated small animal system (Vevo 2100, Visual Sonics, Canada, now Fujifilm) under light general anaesthesia (0.5–2% isoflurane in O₂) in a warm environment to keep body temperature stable. Cardiac dimensions and function were assessed in long and short parasternal axis and apical views. Mean values were taken from at least three images in 2D and M-mode. The experiment and analysis were performed in a blinded fashion, and the analysis was performed by a second blinded observer.

Transmembrane action potential recordings

Transmembrane action potentials were recorded from isolated, superfused LA using floating glass microelectrodes (resistance 15–30 M Ω) filled with 3 M KCl (Holmes et al., 2016; Syeda et al., 2016; Yu et al., 2014). Preparations were paced incrementally from 1000 to 80 ms. Voltage was digitized at 20 kHz and was unfiltered. The trans-

membrane action potentials used for analysis were after 200 stimulations to allow for sufficient rate adaptation.

RNA isolation, sequencing and analysis

Left and right atrial tissue samples were collected from excised hearts after quick perfusion to rinse out the remaining blood. Total RNA from each atrium was extracted using the Direct-zol RNA MiniPrep kit (Zymo Research, USA). RNA integrity number (RIN) values (accepted only if higher than seven) were checked using the Bioanalyzer RNA 6000 Nano Kit (Agilent, USA). Messenger RNA enrichment and subsequent complementary DNA NGS library preparation was completed for individual atrial samples using a NEBNext Poly(A) mRNA Magnetic Isolation Module and Ultra II Directional RNA Library Prep Kit for Illumina (New England BioLabs, UK). The next generation sequencing (NGS) library size distribution was determined by using the Bioanalyzer High Sensitivity DNA Kit (Agilent, USA) and quantified using the KAPA Library Quantification Kit (Roche, Switzerland). Equimolar pooled libraries were sequenced by 75 cycles in a single read mode on the NextSeq 500 System (v.2.5 Chemistry, Illumina). RNA-seq FASTQ files were aligned on HISAT2 (v.2.1.0) using Ensembl Mus Musculus reference GRCm38 (Kim, Paggi, et al., 2019; Zerbino et al., 2018). Aligned reads were counted using HTseq v.0.11.2 (Anders et al., 2015). Required transformations through different RNA-seq analysis steps were done using Samtools v.1.4 (Li et al., 2009). Differential expression was obtained using DESeq2 in R (Love et al., 2014) (<http://www.R-project.org/>, R 3.4.1). Ensembl IDs were transformed to gene symbols using BioTools (https://www.biotoools.fr/mouse/ensembl_symbol_converter, accessed 28 February 2020).

Data will be made publically available at <https://www.ncbi.nlm.nih.gov/geo/>.

Protein quantification

Snap-frozen murine left atria were placed in RIPA lysis buffer (Roche, USA) supplemented with protease inhibitor cocktail tablets (Complete Mini, Roche) and homogenized using 5 mm steel beads (Qiagen, Germany) and the Mini-BeadBeater-8 (BioSpec Products; 6 × 10–15 s bursts). Snap-frozen murine right ventricles were ground to fine powder and resuspended in LB1 containing (mM): Tris-base, 50 (pH 7.5); EDTA, 2; EGTA, 5; DTT, 5; and 0.05% digitonin, in addition to protease and phosphatase inhibitors. Pellets of centrifuged homogenates (17,000 g, 30 min) were resuspended in LB2 (LB1 + 1% Triton X-100) and centrifuged again. Forty-five micrograms of protein from the supernatants comprising the membrane-enriched fractions were used

for SDS-PAGE and semi-dry blotting. Membranes were blocked in 5% milk in TBS–Tween and antibodies were diluted in 0.5% milk (Connexin 43, Thermo Scientific, 13-8300, 1:250; Nav1.5, Cell Signalling Technology, 14421 D9J7S, 1:1,000; Na⁺-K⁺-ATPase, Cell Signalling Technology, 3010, 1:1,000) or 5% milk (Plakoglobin, BD TL, clone 15, 610254, 1:2,000; Calnexin, Abcam, ab22595, 1:2,000) in TBS–Tween. Protein–antibody–horseradish peroxidase complexes were visualized using ECL substrates on a ChemiDoc Imaging System (Bio-Rad, USA). Samples were run twice, and average chemiluminescence values were used for comparison.

Left atrial cardiomyocyte isolation

Hearts were mounted onto a Langendorff apparatus and perfused with the following three solutions, equilibrated with 100% O₂: (i) HEPES-buffered modified Tyrode solution containing (mM): NaCl, 145; KCl, 5.4; CaCl₂, 1.8; MgSO₄, 0.83; Na₂HPO₄, 0.33; HEPES, 5; and glucose, 11 (pH 7.4, NaOH) for 5 min; (ii) Ca²⁺-free Tyrode solution × 5 min; and (iii) Tyrode enzyme solution containing 20 µg/ml Liberase (Roche, USA) or a collagenase/protease mix [640 µg/ml collagenase type II, 600 µg/ml collagenase type IV and 50 µg/ml protease (Worthington, USA)], 20 mM taurine and 30 µM CaCl₂ for 15–20 min. The LA was removed and placed into a high-K⁺ modified Kraft–Bruhe (KB) solution containing (mM): D,L-potassium aspartate, 10; L-potassium glutamate, 100; KCl, 25; KH₂PO₄, 10; MgSO₄, 2; taurine, 20; creatine, 5; EGTA, 0.5; HEPES, 5; 0.1% bovine serum albumin (BSA, Sigma); and glucose, 20 (pH 7.2, KOH). The LA was dissected into small strips, and then cells were released by gentle trituration with fire-polished glass pipettes (1–2 mm in diameter). Cells to be used for patch-clamp experiments were gradually reintroduced to Ca²⁺ over a period of 2 h to reach a final concentration of 1.8 mM. All experiments were performed within 4–8 h of isolation.

Sodium current recordings

Isolated atrial cells were plated on laminin-coated coverslips and superfused at 3–4 ml/min at 22 ± 0.5°C with a low-sodium external solution containing (mM): NaCl, 10; C₅H₁₄ClNO, 130; HEPES, 10; CaCl₂, 1.8; MgCl₂, 1.2; NiCl₂, 2; and glucose, 10, pH 7.4 (CsOH). Peak sodium current (*I*_{Na}) was recorded in voltage-clamp mode using borosilicate glass pipettes (tip resistance 1.5–2.5 MΩ). The internal pipette solution contained (mM): NaCl, 5; CsCl, 115; HEPES, 10; EGTA, 10; MgATP, 5; MgCl₂, 0.5; and TEA, 20, pH 7.2 (CsOH). Currents were digitized at 50 kHz and low-pass filtered at 20 kHz. Series resistance was compensated between 60 and 80%. Experiments were terminated if series resistance increased abruptly or was >10 MΩ (usually 4–8 MΩ).

Current–voltage relationships were examined using 100 ms step depolarizations over test potentials ranging from -95 to $+40$ mV, in 5 mV increments, from a holding potential of -100 mV. Current–voltage curves were fitted using the modified Boltzmann equation: $I_{\text{Na}} = G_{\text{max}}(V_m - V_{\text{rev}})/\{1 + \exp[(V_{0.5} - V_m)/k]\}$, where I_{Na} is the current density at an equivalent test potential (V_m), G_{max} is the peak conductance (in nanosiemens), V_{rev} is the reverse potential, $V_{0.5}$ is the membrane potential at 50% current activation and k is the slope constant (Ackers-Johnson et al., 2016; Spencer et al., 2001). Time-dependent peak I_{Na} recovery kinetics were evaluated using standard 20 ms P1–P2 pulse protocols (-100 to -30 mV) with increasing time delay ranging from 1 to 100 ms. Measurements of steady-state inactivation of I_{Na} were made by applying 500 ms prepulses ranging from -120 to -40 mV in 5 mV increments prior to the test potential (-30 mV for 100 ms). Individual atrial cell capacitance was calculated by integrating the cellular capacitance current elicited by 10 mV depolarization from a holding potential of -80 mV.

Analysis of atrial cell diameter and extracellular matrix composition

Hearts were isolated, and coronary arteries were cleared of blood using KH buffer before being snap-frozen in optimal cutting temperature (OCT) compound. For cell diameter analysis, 10- μm -thick atrial sections were stained with FITC-conjugated wheat germ agglutinin (1:1,000) and imaged on a Leica DM6000 B fully automated fluorescence microscope (Leica Microsystems, Germany) with a $\times 40$ objective. Scaled images were extracted using the LASX (Leica Application Suite X, Leica Microsystems, Germany) imaging suite, and cell diameter and endomyocardial fibrosis were quantified from sections using the JavaCyte ImageJ plugin (Winters et al., 2020).

Super-resolution microscopy and $\text{Na}_v 1.5$ cluster analysis

Left atrial cells were plated on 10-mm-diameter laminin-coated coverslips (35 mm dish, 1.5# coverglass, MatTek, USA) and then fixed in 4% paraformaldehyde for 90 min to ensure maximal immobilization of cellular proteins. Cells were permeabilized with a solution of 0.1% Triton in PBS for 5 min and blocked in a solution of 5% BSA in PBS for 60 min. The primary polyclonal rabbit anti- $\text{Na}_v 1.5$ antibody (ASC-005, Alomone Laboratories, Israel; 1:50) was diluted in blocking solution and incubated overnight at 4°C . Cells were washed three times in PBS, blocked again for 30 min, then incubated in secondary antibody fragment [F(ab')₂-goat anti-rabbit IgG, Alexa Fluor 647, A212-56, 1:1,000;

ThermoFisher Scientific, USA] for 90 min at room temperature. Direct stochastic optical reconstruction microscopy (dSTORM) experiments were performed on a NIKON Eclipse Ti inverted N-STORM microscope equipped with a NIKON APO 100 \times 1.49 NA total internal reflection fluorescence (TIRF) oil-immersion objective. Laser illumination was provided using 405 nm (20 mW), 491 nm (100 mW), 561 mW (100 mW) and 640 nm (200 mW) solid-state lasers. A NIKON Perfect Focus System (PFS) ensured minimal lateral drift during acquisition. Immunolabelled samples were imaged in 0.5 mg/ml glucose oxidase, 40 $\mu\text{g}/\text{ml}$ catalase, 10% w/v glucose and 100 mM MEA in PBS, pH 7.4 to induce Alexa 647 blinking. During dSTORM acquisition, the sample was continuously illuminated at 640 nm for 20,000 frames; fluorescence emission was filtered through a single-band far-red emission filter (MBE47200 N-STORM cube) and detected using an Andor iXon Ultra DU897 EMCCD camera (256 \times 256 pixels, 160 nm effective pixel size and 9.2 ms exposure time). The angle of illumination and the z -depth were kept as consistent as possible across different samples. Samples were maintained in an OKO environmental chamber at 27°C for maximum system stability during imaging.

Fluorescence detections were localized in ThunderSTORM (Ovesny et al., 2014) using default settings for the localization step. Post-localization, the samples were subjected to drift correction (cross-correlation), filtering for localizations with a spatial uncertainty < 40 nm, duplicate removal (distance threshold 75 nm) and merging (performed with a maximum distance of 75 nm; maximum off frames 1; and maximum frames per molecule 0).

Depending on the overall number of blinking events in a sample, either 20,000 or 5,000 of the post-processed images were subjected to cluster analysis. Owing to variability in blinking events across different imaging sessions, resulting cluster parameters from each group were normalized to the mean of the WT control group acquired during the same imaging session.

Before cluster analysis, we checked the spatial distribution of membrane-localized detections at the cell end *versus* cell middle in $1\ \mu\text{m} \times 1\ \mu\text{m}$ regions each. Given that the distribution of localizations across groups was not different between the two regions and in order to use as many data points as possible, we performed cluster analysis for the whole region imaged.

For cluster analysis, we used a topological analysis tool (Pike et al., 2020) with codes customized to cardiomyocyte images in an R environment and the following set parameters: $r = 40$ nm, threshold = 10 and minimal number of detections per cluster = 10. Before cluster analysis, only data points within the cell area were selected using the normalized Ripley's K -function [H -function, $H(r) = L(r) - r$], with a set linking distance of $r = 1\ \mu\text{m}$,

and only points with $H(r) > 0$, indicating a non-dispersed spatial distribution, were included [background will be randomly distributed, hence $H(r) < 0$]. The minimum area to be detected as a 'cell' was set to $15 \mu\text{m}^2$. Final super-resolution rendered images were achieved by applying a normalized Gaussian with magnification 50 and the lateral uncertainty set to the calculated uncertainty of the localization for each blink (20 nm). Cell area selection and cluster map images for visualization were generated using MATLAB.

Statistics

All experiments and analyses were performed blinded to genotype and treatment. Data from murine studies were first subjected to outlier analysis, the ROUT method, based around a false-discovery rate, where $\alpha = 0.01$ and outliers were removed (Prism v.8, GraphPad Software, USA). Associations between categorical variables were analysed by Fisher's exact test. Significance between groups for normally distributed data was taken as $P < 0.05$, ordinary one-way or two-way (repeated)-measures ANOVA, with Bonferroni's *post hoc* test, as appropriate. Non-normally distributed data were subjected to the Kruskal–Wallis test with a significance level of $P < 0.05$ and Dunn's *post hoc* test (Prism v.8). Data are presented as the mean \pm SD unless stated otherwise.

Ethical approval

Ethical approval for analysis of clinical data from Inherited Cardiac Conditions Clinic at the University Hospital Queen Elizabeth, Birmingham, was granted by the local department of research ethics at the Queen Elizabeth Hospital. Given that this observational study in patients receiving standard National Health Service care was performed as part of an audit [(CARMS)-16044, 17734], the clinical audit committee by Birmingham Children's Hospital Clinical Audit and Effectiveness Lead/University Hospitals Birmingham waived the need of informed consent (Aljehani et al., 2023).

All animal procedures were approved by the UK Home Office (PPL number 30/2967 and PFDAAF77F) and by the institutional review board of University of Birmingham, UK. All animal procedures conformed to the guidelines from Directive 2010/63/EU of the European Parliament on the protection of animals used for scientific purposes.

Results

Atrial arrhythmias and ECG changes in definite ARVC patients

The clinical cohort studied (Aljehani et al., 2023) consisted of 146 patients with suspected cardiomyopathy;

97 were identified as 'non-definite' ARVC cases and 49 as 'definite' ARVC, i.e. presenting with a complete phenotype according to the 2010 TFC (Marcus et al., 2010). Semi-automated analysis of available digital ECG lead II recordings focusing on atrial parameters (Fig. 1A) showed PR interval prolongation, increased P wave duration and increased P wave area in the advanced, definite disease stage (Fig. 1B). Non-definite ARVC patients exhibited no difference in the analysed P wave parameters compared with unaffected control subjects. The mean age of the patients at the time of ECG analyses was not different between the groups (Table 1; 42 ± 18 years for non-definite vs. 43 ± 18 years for definite, $P = 0.743$). There was a significant association between male sex and ARVC diagnosis type (Fig. 1C and Table 1; 43% male amongst non-definite vs. 73% male amongst definite patients, $P = 0.007$). Twenty-four per cent of definite ARVC patients experienced AF and/or flutter [summarized as 'atrial arrhythmia (AA)'], compared with only 3% of the non-definite ARVC patients (Table 1 and Fig. 1C). The weighted mean of AA prevalence from a meta-analysis of published registries was 16% (Fig. 1D).

5 α -Dihydrotestosterone causes general and cardiac growth response in mice

To study increased androgen exposure and desmosomal instability jointly in atria, Plako^{+/-} mice and WT littermates were subjected to chronic DHT treatment over 6 weeks (refer to Fig. 2 for an overview scheme).

Treatment led to a 3- to 4-fold increase in serum DHT concentration in both genotypes compared with controls (Ctr) (Fig. 3A). Treatment with DHT increased body weight (Fig. 3B) and seminal vesicle mass/tibia length ratio (Table 2) and led to left ventricular hypertrophy in Plako^{+/-} animals (Table 2). The DHT caused a mild atrial growth response. Atrial weight/tibia length ratio (Fig. 3C) and atrial area/tibia length ratio (Fig. 3D) were increased in Plako^{+/-} mice after DHT exposure.

Exploratory RNA sequencing analysis confirmed ~50% reduction in atrial plakoglobin (*Jup*) expression in Plako^{+/-} compared with WT animals (Fig. 3E). A reduction in atrial plakoglobin was also confirmed at the protein level (Fig. 2). In control hearts, gene expression patterns did not differ markedly between genotypes (data not shown). Chronic DHT exposure resulted in significant transcriptional changes in atria of both WT and Plako^{+/-} mice: DHT activated expression of genes associated with muscle growth (e.g. *Igf1*, *Mtpn* and *Myocd*) and also immune (e.g. *C7*, *Tlr3* and *Tlr4*) and pro-fibrotic response genes (e.g. *Col1a1*, *Col3a1*, *Srf* and *Lox*; Fig. 3F), confirming the increased atrial weight and atrial area/tibial length ratio. Transcriptional changes were induced to a similar extent

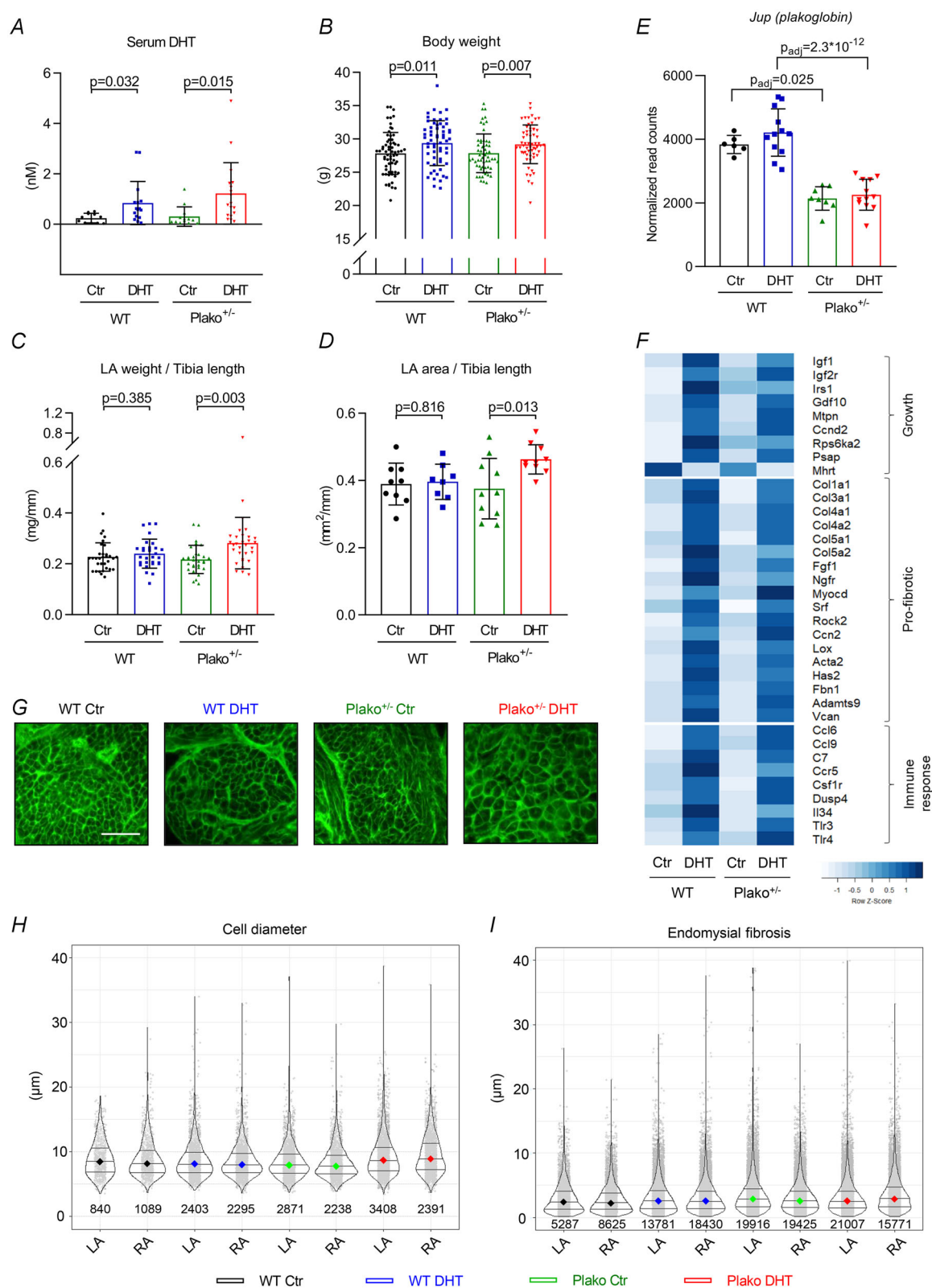


Figure 3. Systemic and atrial growth response and atrial gene expression profiles

A and **B**, serum 5 α -dihydrotestosterone (DHT) concentration (**A**; $n = 11$ – 18 mice per group) and body weight (**B**; $n = 48$ – 54 mice per group) are increased after DHT treatment. **C**, **D**, left atrial (LA) weight to tibia length ratio (**C**; $n = 29$ – 32 atria per group) and LA unfolded area (**D**; $P < 0.05$, two-way ANOVA) measured from optical mapping raw images is significantly increased in Plako^{+/−} subjected to DHT (*post hoc* Student's unpaired *t* test, *P*-values indicated

on graph, $n = 8-10$ atria per group). *E*, normalized read counts of the plakoglobin gene *Jup* from RNA sequencing analysis, confirming ~50% reduction of expression in heterozygous knockout ($Plako^{+/-}$) animals in both left ($n = 3-6$ /group) and right atria (RA; $n = 3-6$ per group; Benjamini Hochberg-corrected P -values from DESeq2 reported on graph). *F*, selected genes significantly regulated (Benjamini Hochberg-corrected P -value from DESeq2 < 0.05) by DHT exposure in at least one of the genotypes. The DHT treatment leads to atrial growth, pro-fibrotic and immune response gene expression. $n =$ WT Ctr, 3 LA + 3 RA; WT DHT, 6 LA + 6 RA; $Plako^{+/-}$ Ctr, 4 LA + 4 RA; $Plako^{+/-}$ DHT, 6 LA + 6 RA. *G-I*, example LA sections (*G*) stained with FITC-conjugated wheat germ agglutinin (lectin, $\times 400$ magnification; scale bar represents $20 \mu m$) for automated quantification of cell diameter (*H*) and endomysial fibrosis (*I*; cell-to-cell distance) in both LA and RA. Individual measurement's data points (light grey) with violin plots including medians (colour coded per group) and the interquartile range are shown. Numbers indicate total measured cells/cell-to-cell distances. Linear mixed modelling revealed no significant differences between genotype or treatment groups. Genes are as follows: *Acta2*, smooth muscle (α)-2 actin; *Adams9*, ADAM metalloproteinase with thrombospondin type 1 motif 9; *C7*, complement C7; *Ccn2*, connective tissue growth factor; *Cnd2*, cyclin D2; *Ccr5*, C-C motif chemokine receptor 5; *Col1a1/3a1/4a1/4a2/5a1*, collagen type 1 alpha 1/3 alpha 1/4 alpha 1/4 alpha 2/5 alpha 1; *Csf1r*, colony stimulating factor 1 receptor; *Dusp4*, dual specificity phosphatase 4; *Fbn1*, fibrillin 1; *Fgf1*, fibroblast growth factor 1; *Gdf10*, growth differentiation factor; *Has2*, hyaluronan synthase 2; *Igf1*, insulin-like growth factor 1; *Igf2r*, insulin-like growth factor 2 receptor; *Il34*, interleukin 34; *Irs1*, insulin receptor substrate 1; *Lox*, lysyl oxidase; *Mhrt*, myosin heavy chain associated RNA transcript; *Mtpn*, myotrophin; *Myocd*, myocardin; *Ngfr*, nerve growth factor receptor; *Psap*, prosaposin; *Rock2*, rho associated coiled-coil containing protein kinase 2; *Tlr3*, toll like receptor 3; *Tlr4*, toll like receptor 4.

in left and right atria. However, atrial cardiac myocyte diameter and endomysial collagen deposition were not significantly different between genotypes after DHT treatment, as quantified in semi-automated histological analysis (Fig. 3*H* and *I*).

5 α -Dihydrotestosterone induces atrial ECG changes in plakoglobin-deficient mice

To check whether atrial ECG changes observed in definite ARVC patients are also present in the murine model, ECGs were recorded from conscious mice after DHT treatment or placebo control. Both PR interval and P wave duration exhibited mild but significant prolongation in $Plako^{+/-}$ animals exposed to DHT compared with WT littermates exposed to DHT (Fig. 4*A* and *B*). Echocardiographic assessment of the left atrial diameter *in vivo* revealed ventricular but not atrial hypertrophy (Table 2 and Fig. 4*C* and *D*).

5 α -Dihydrotestosterone causes atrial conduction slowing in heterozygous plakoglobin-deficient hearts

Chronic DHT exposure slowed conduction in $Plako^{+/-}$ but not WT atria (Fig. 5*A-C*). The reduction in

conduction velocity in $Plako^{+/-}$ DHT atria was more pronounced at higher pacing frequencies. The $Plako^{+/-}$ atria exposed to DHT exhibited an overall prolongation of 95% atrial activation times and increased beat-to-beat activation variability compared with WT Ctr and $Plako^{+/-}$ Ctr atria (Fig. 5*D-F*). Intact hearts from $Plako^{+/-}$ mice exposed to DHT showed a non-significant trend towards a more frequent occurrence of atrio-ventricular block in *ex vivo* Langendorff experiments (Fig. 5*G*).

5 α -Dihydrotestosterone reduces atrial action potential amplitude and rate of depolarization in heterozygous plakoglobin-deficient atria

The intracellular microelectrode technique was used to record transmembrane action potentials from paced, superfused atria (Fig. 6*A* and *B*). Paced atria isolated from $Plako^{+/-}$ DHT mice showed longer activation times (Fig. 6*C*). Action potential amplitude was reduced in $Plako^{+/-}$ DHT left atria, as was the peak rate of depolarization (dV/dt_{max}), both indicative of sodium current impairment (e.g. 120 ms pacing CL WT Ctr, 118 ± 5 V/s; WT DHT, 120 ± 7 V/s; $Plako^{+/-}$ Ctr, 116 ± 4 V/s; $Plako^{+/-}$ DHT, 89 ± 5 V/s; Fig. 6*D* and *E*). Chronic DHT

Table 1. Arrhythmogenic right ventricular cardiomyopathy (ARVC) patient and control characteristics

Characteristic	Control subjects ($n = 12$)	Non-definite ARVC ($n = 97$)	Definite ARVC ($n = 49$)	P -value*
Age at last follow-up, mean \pm SD (years)	38 ± 14	42 ± 18	43 ± 16	0.743
Male, n (%)	7 (58)	42 (43)	36 (73)	0.007
Atrial fibrillation/flutter, n (%)	–	3 (3)	12 (24)	0.0001
		♂, 2 ♀, 1	♂, 8 ♀, 4	

* Non-definite versus definite, Fisher's exact test.

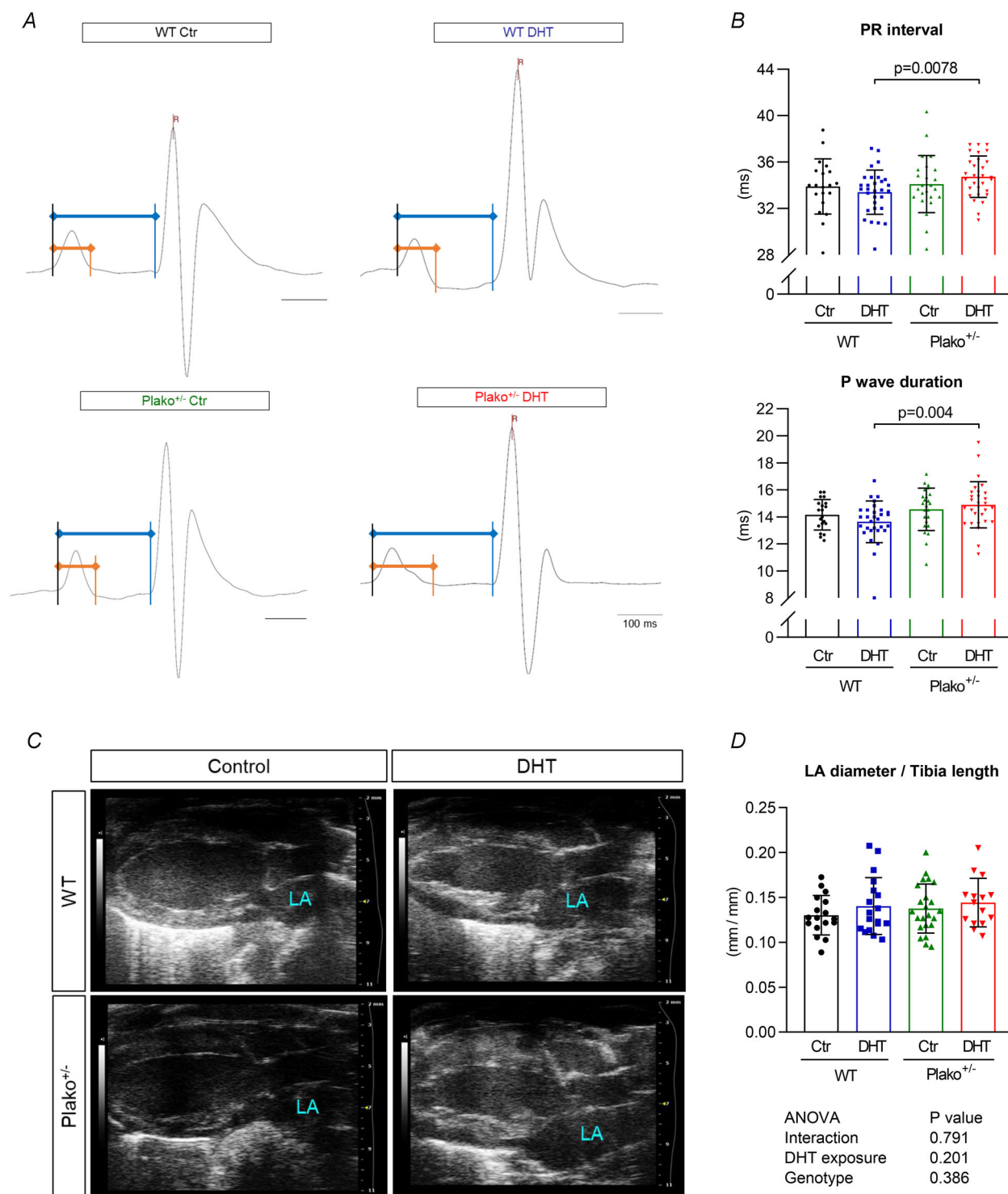


Figure 4. Murine atrial ECG and echocardiography parameters

A, exemplary ECG recordings in conscious mice. Shown are compound potentials averaged from 20 subsequent cardiac cycles. The PR interval (blue) and monophasic part of the P wave (orange) are marked. B, PR interval ($n = 30\text{--}34$ mice per group) and P wave duration ($n = 20\text{--}30$ mice per group) are prolonged in $\text{Plako}^{+/-}$ DHT compared with WT DHT (two-way ANOVA, $P < 0.05$ with *post hoc* Student's unpaired *t* test; *P*-values are indicated on graphs). C, example echocardiographic images obtained in parasternal long axis view, displayed during systole (atrial diastole). D, LA diameter from echocardiography normalized to tibia length ($n = 15\text{--}23$ mice per group). Abbreviations: DHT, 5α -dihydrotestosterone; LA, left atrium; WT, wild type.

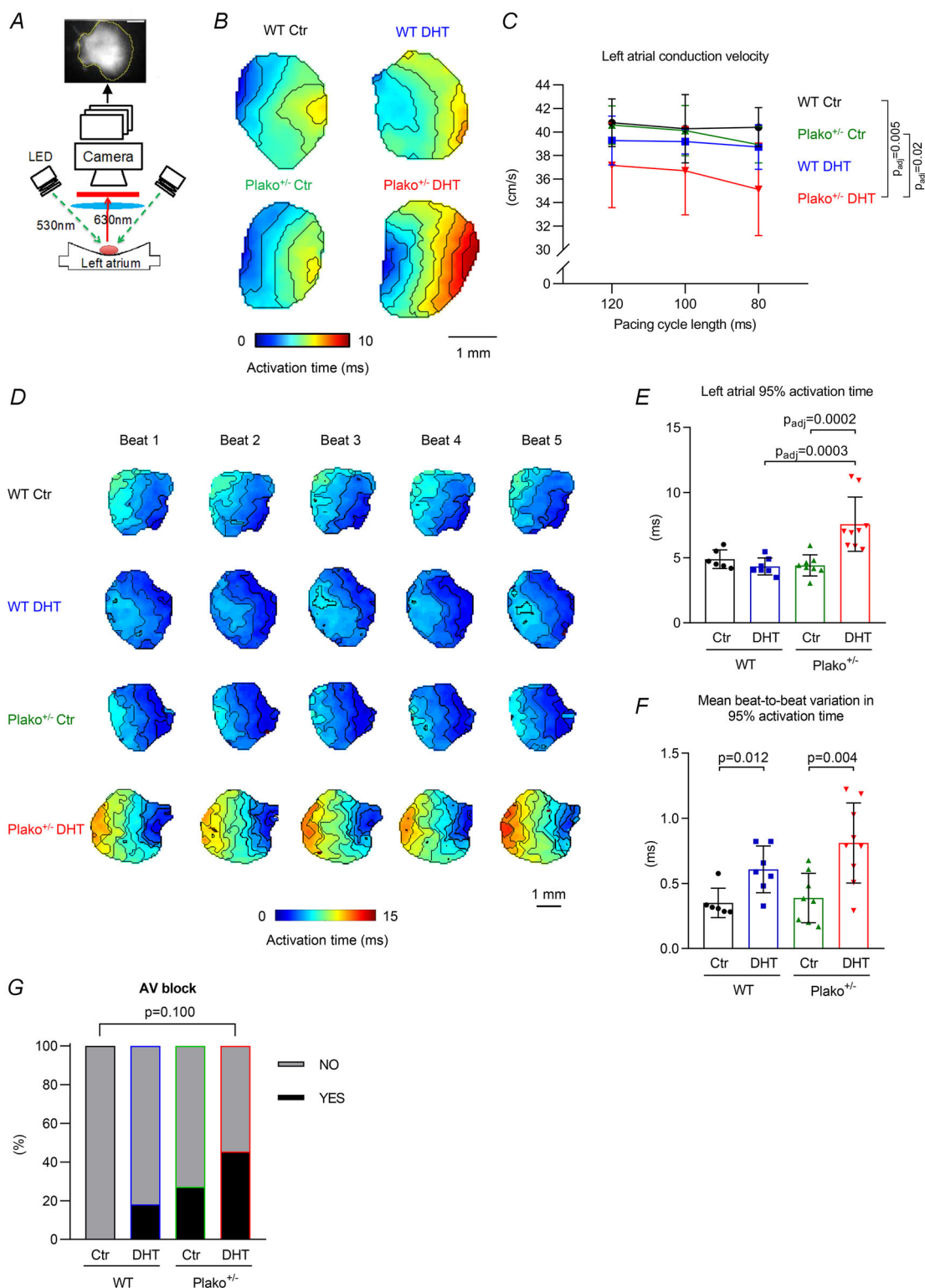


Figure 5. Left atrial area, conduction velocity and activation time variation

A, experimental set-up for optical mapping of isolated LA. B, exemplary isochronal activation maps of LA at 100 ms pacing CL (averaged). C, both heterozygous deletion of plakoglobin (Plako^{+/-}) and DHT exposure have a significant effect on LA conduction velocity ($P < 0.05$, two-way repeated measures ANOVA), but it is significantly decreased only in LA of Plako^{+/-} DHT animals (Bonferroni-adjusted *post hoc* test, across all CLs, $n = 8-9$ LA per group). D, example individual beat activation maps taken from the final five beats of a train of 50 pulses at 80 ms pacing

CL. *E*, both genotype and DHT exposure have a significant effect on beat-averaged 95% LA activation times. *F*, DHT treatment has a significant effect on mean beat-to-beat variation in 95% activation times calculated from the final 10 beats of a train of 50 pulses at 80 ms CL (two-way ANOVA with *post hoc* analysis as appropriate, *P*-values indicated). Individual data points denote a single LA. Number of LA: WT Control, 6; WT DHT, 7; Plako^{+/-} Control, 8; Plako^{+/-} DHT, 9. *G*, percentage of hearts with AV block occurring during *ex vivo* Langendorff perfusion experiments. Number of hearts: WT Control, 6; WT DHT, 11; Plako^{+/-} Control, 11; Plako^{+/-} DHT, 11. *D*, LA diameter from echocardiography normalized to tibia length (*n* = 15–23 mice per group). Abbreviations: AV, atrio-ventricular; CL, cycle length; DHT, 5 α -dihydrotestosterone; LA, left atrium; WT, wild type.

exposure did not modify action potential duration (APD), beat-averaged left atrial optical APD90 or beat-to-beat APD90 variability (data not shown).

5 α -Dihydrotestosterone decreases peak sodium current density in heterozygous plakoglobin-deficient atrial cardiac myocytes

To examine mechanisms underlying alterations in action potential morphology and conduction in Plako^{+/-} DHT atria, whole-cell patch-clamp experiments were performed, monitoring peak sodium current (I_{Na}) amplitude and kinetics. Peak whole-cell I_{Na} density was decreased by ~20% in Plako^{+/-} atrial cells after DHT exposure (Fig. 7A–C). Left atrial cell capacitance was elevated by DHT exposure in both WT and Plako^{+/-}, but not different between the genotypes (Fig. 7D). There was a considerable spread of individual cell capacitance in DHT-exposed groups, indicative of variable degrees of hypertrophy. Activation kinetics were consistent between all groups (V_{50} activation, WT Ctr, -43 ± 1 mV; WT DHT, -46 ± 1 mV; Plako^{+/-} Ctr, -46 ± 1 mV; Plako^{+/-}

DHT, -46 ± 2 mV). Exposure to DHT caused a leftward shift in steady-state inactivation kinetics in Plako^{+/-} (Fig. 7E). The 50% recovery time (P_{50}) from inactivation was significantly longer in the Plako^{+/-} DHT, suggestive of a delayed rate of sodium channel recovery (Fig. 7F).

Expression of *Scn5a*, encoding for the alpha subunit of Na_v1.5, was not different between groups (Fig. 7G). Relative protein expression of Na_v1.5 assessed by immunoblot in membrane-enriched fractions revealed only a non-significant trend towards reduction in the Plako^{+/-} DHT compared with the WT DHT group (Fig. 7H). Membrane connexin 43 followed the same pattern (Fig. 7H).

Na_v1.5 cluster depletion in Plako^{+/-} atrial cardiac myocytes following DHT exposure

Protein quantification of ion channels by western blot could neither prove nor disprove a reduction in Na_v1.5 in membrane fractions of cardiac tissue (Fig. 7H). To define a molecular cause of I_{Na} density depletion in Plako^{+/-} DHT atrial cardiac myocytes, we examined Na_v1.5 organization

Table 2. Phenotypic characteristics of the Plako^{+/-} murine model and wild type littermates

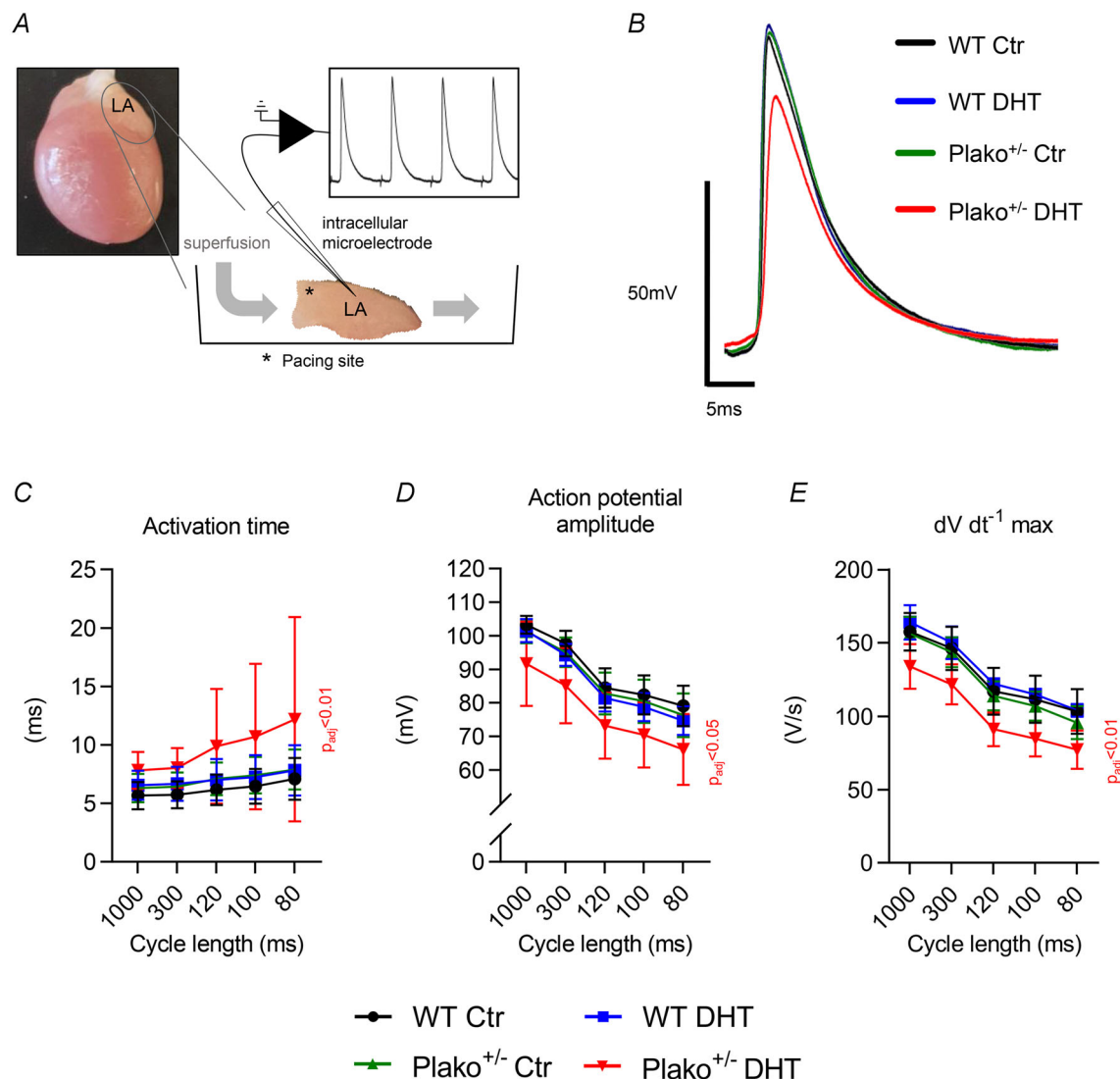
Characteristic	WT control	WT DHT	<i>P</i> -value	Plako ^{+/-} control	Plako ^{+/-} DHT	<i>P</i> -value
Age at terminal experiment (weeks) (<i>n</i> = 59–67)	16.5 \pm 0.2	16.7 \pm 0.2	n.a.	16.0 \pm 0.2	16.6 \pm 0.2	n.a.
Body weight (g) (<i>n</i> = 59–65)	27.9 \pm 0.4	29.4 \pm 0.4	0.010	27.9 \pm 0.4	29.2 \pm 0.4	0.014
Serum DHT (nM) (<i>n</i> = 11–18)	0.25 \pm 0.06	0.85 \pm 0.21	0.032	0.31 \pm 0.11	1.22 \pm 0.29	0.015
Left atrial weight:tibia length (mg/mm) (<i>n</i> = 29–32)	0.23 \pm 0.01	0.24 \pm 0.01	0.385	0.22 \pm 0.01	0.28 \pm 0.02	0.003
Right atrial weight:tibia length (mg/mm) (<i>n</i> = 28–32)	0.25 \pm 0.01	0.29 \pm 0.01	0.044	0.26 \pm 0.02	0.30 \pm 0.03	0.172
Seminal vesicle weight:tibia length (mg/mm) (<i>n</i> = 39–45)	6.0 \pm 0.4	6.0 \pm 0.3	0.909	5.5 \pm 0.2	6.5 \pm 0.3	0.019
Murine echocardiography (light anaesthesia, mean heart rate 390–440 beats/min)						
Heart rate (beats/min) (<i>n</i> = 18–28)	411 \pm 3	415 \pm 3	0.365	413 \pm 3	414 \pm 3	0.751
Left atrial diameter:tibia length (mm/mm) (<i>n</i> = 15–23)	0.130 \pm 0.005	0.140 \pm 0.007	0.285	0.138 \pm 0.006	0.144 \pm 0.007	0.468
Left ventricular mass:tibia length (mg/mm) (<i>n</i> = 18–28)	5.4 \pm 0.3	5.5 \pm 0.3	0.903	4.9 \pm 0.2	6.0 \pm 0.3	0.007
Left ventricular ejection fraction (%) (<i>n</i> = 18–28)	43 \pm 3	50 \pm 3	0.074	47 \pm 2	45 \pm 3	0.632

Data presented as the mean \pm SEM; *n* = number of animals per group. The *P*-values for differences between control and DHT groups are reported. Abbreviations: DHT, 5 α -dihydrotestosterone; WT, wild type.

at the super-resolution level using dSTORM. Owing to the high variability in T-tubule density between different atrial cells, we focused on $\text{Na}_V1.5$ channels located within ~ 200 nm of the contact cell surface membrane by using TIRF/HILO. Exemplary super-resolution images of $\text{Na}_V1.5$ detections and characteristic cluster maps are shown in Fig. 8A.

At the $\text{Plako}^{+/-}$ DHT atrial cardiac myocyte membranes, fewer $\text{Na}_V1.5$ detections were observed compared with WT DHT (Fig. 8B). Of the total detections,

the proportion present in distinct $\text{Na}_V1.5$ clusters was significantly lower in the $\text{Plako}^{+/-}$ DHT compared with WT DHT cardiac myocytes (Fig. 8C). Characteristics of identified $\text{Na}_V1.5$ clusters, i.e. cluster density and cluster area, were similar in all four groups (data not shown). The 95% confidence intervals generated from our murine WT Ctr LA experiments suggest a range of 3×10^{-3} to 4×10^{-3} $\text{Na}_V1.5$ channels/ nm^2 cluster (Fig. 8D; both mean and median at 3×10^{-3} channels/ nm^2 cluster), resulting in an estimated nearest-neighbour distance of 20 nm.



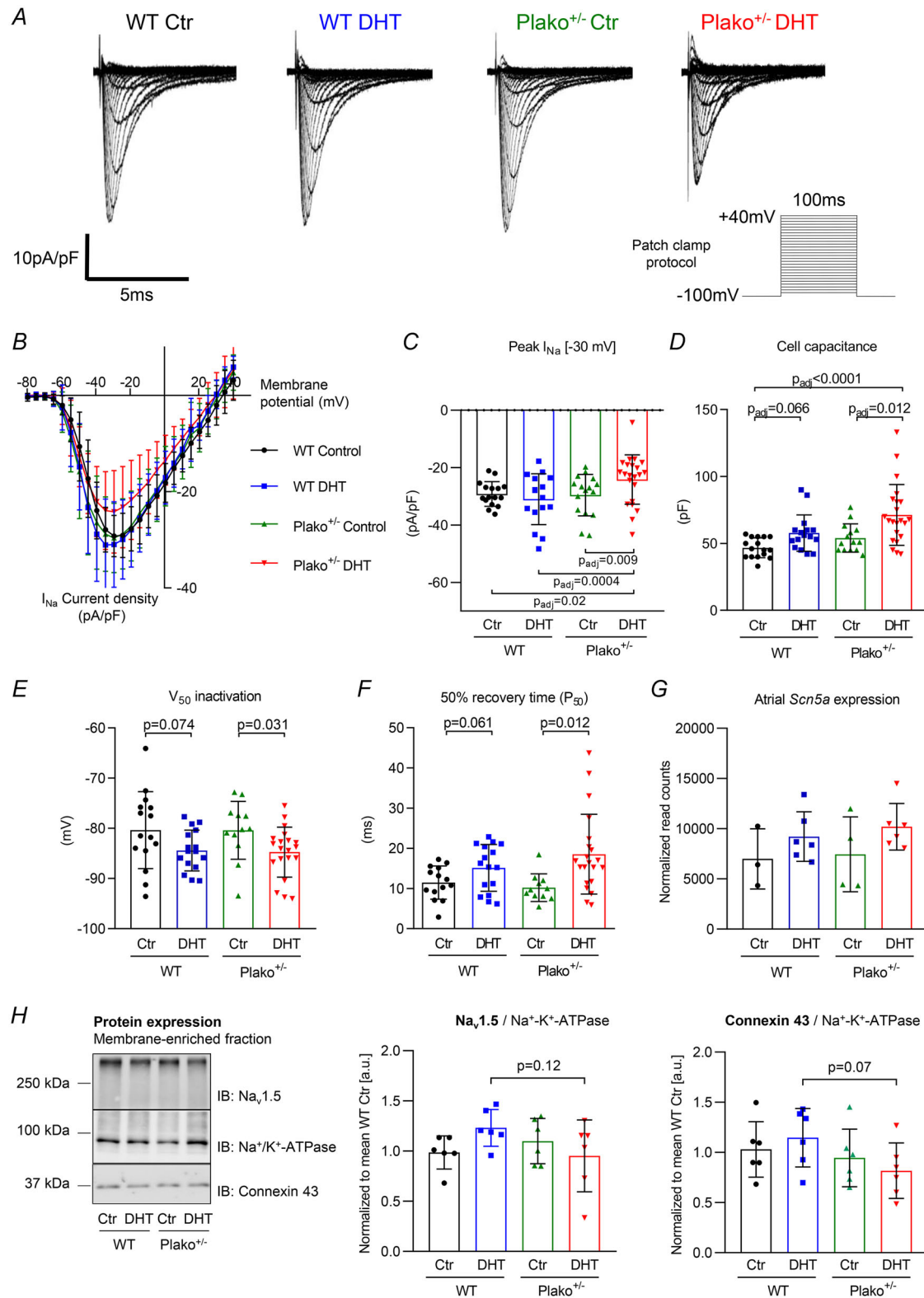


Figure 7. Atrial cardiomyocyte sodium current, cell capacitance and cardiac expression of membrane sodium channel and connexin

A, representative atrial whole-cell peak Na⁺ current (I_{Na}) traces measured at test potentials of -100 to +40 mV. B, mean current-voltage relationships. C, peak sodium current density at -30 mV membrane potential. Plako^{+/-} DHT atrial cardiomyocytes have reduced I_{Na} density (two-way repeated-measures ANOVA with Bonferroni *post hoc*

analysis). *D*, both genotype and DHT treatment show a significant effect on individual cell capacitance (two-way ANOVA, $P < 0.05$). Bonferroni-corrected *post hoc* analysis shows a significant increase in cell capacitance by DHT compared with Ctr in both genotypes. Cell capacitance is highest in atrial cardiomyocytes from Plako^{+/-} DHT. *E*, mean V_{50} values for steady-state inactivation of sodium channels (two-way ANOVA, $P < 0.05$). Results of *post hoc* Student's unpaired *t* test are indicated on the graph. *F*, 50% sodium channel recovery times (P_{50}) for each group (two-way ANOVA, $P < 0.05$). Results of *post hoc* Student's unpaired *t* test are indicated on the graph. Plako^{+/-} LA DHT-treated cells have delayed recovery. In *B–F*, WT Ctr, $n = 14$ cells, $N = 5$ atria; WT DHT, $n = 16$ cells, $N = 5$ atria; Plako^{+/-} Ctr, $n = 11$ cells, $N = 4$ atria; and Plako^{+/-} DHT, $n = 21$ cells, $N = 5$ atria. *G*, normalized read counts of sodium channel transcript *Scn5a* in atria obtained from RNA sequencing analysis ($n = 3–6$ atria per group). *H*, protein expression in membrane-enriched cardiac tissue fractions: left, example IBs; and right, quantification of relative Na_v1.5 and connexin 43 expression normalized to Na⁺-K⁺-ATPase expression ($n = 6$ right ventricles per group). Abbreviations: Ctr, control; DHT, 5 α -dihydrotestosterone; IB, immunoblot; LA, left atrium; WT, wild type.

Discussion

Major findings

Our main findings are as follows. First, atrial arrhythmias and P wave changes represent a common clinical observation in patients with ARVC. The cohort studied here presents with a male preponderance amongst definite ARVC patients. Exposure to the potent androgen DHT leads to pro-hypertrophic, pro-fibrotic and inflammatory transcriptional signatures in murine atria. Third, chronic DHT exposure in mice heterozygously deficient for plakoglobin induces atrial changes in the ECG like those observed in ARVC patients. Fourth, increased DHT concentrations together with haploinsufficiency of plakoglobin are associated with a decreased number of membrane-localized Na_v1.5 clusters, reduced atrial sodium current density and atrial conduction slowing.

We report that definite ARVC patients exhibit increased P wave area and prolonged PR interval and P wave duration in the ECG. A phenocopy of these ECG changes is observed in plakoglobin-deficient mice exposed to supraphysiological DHT concentrations. Heterozygous plakoglobin deficiency predisposes cardiac atrial tissue to hypertrophy and a reduction in sodium current density after 6 weeks of exposure to elevated concentrations of DHT, resulting in a decrease in the peak upstroke velocity of the atrial action potential (dV/dt_{\max}), left atrial conduction slowing and increased electrical beat-to-beat variability. Super-resolution microscopy (dSTORM) identified a depletion of Na_v1.5 channels and clusters at atrial cardiomyocyte membranes isolated from Plako^{+/-} DHT-treated mice. This was accompanied by the functional electrophysiological modifications of reduced atrial Na_v1.5 current density and impaired atrial conduction.

The results are likely to capture an early disease stage and underpin the role of plakoglobin in regulating Na_v1.5 channel cellular localization in the LA and in preserving LA electrical integrity in response to stressors, such as pro-hypertrophic DHT exposure.

Patients in the definite ARVC disease stage display a preponderance of male sex, a high prevalence of atrial arrhythmias and P wave changes

One-quarter (24%) of the patients with definite ARVC in our cohort had atrial arrhythmias. Meta-analysis of published studies (between 1991 and 2021) revealed a weighted mean atrial arrhythmia prevalence of 16% amongst a total of 1968 ARVC patients (Table 3). More than 99% of the reported patients were diagnosed with 'definite' ARVC. Male preponderance, with a weighted mean of 66% males, in definite ARVC was a common feature of all screened patient cohorts. Definite ARVC patients were also more likely to be male in the cohort described here (Table 1 and Fig. 1).

Several P wave indices were found to be changed in the ARVC patients with the definite disease stage. P wave duration was prolonged, and P wave area increased in those patients compared with control subjects or non-definite patients, suggesting pathophysiological remodelling. Both P wave prolongation and increased P wave area have been associated with AF or increased AF recurrence (Gorenk et al., 2003; Magnani et al., 2015; Soliman et al., 2009; Weinsaft et al., 2014). Definite ARVC patients displayed longer PR intervals than non-definite patients and control subjects, suggesting attenuated conduction of the atrioventricular node. In line with our results, Baturova et al. (2021) found evidence for ARVC disease progression to be paralleled by changes in the P wave area. Generally, this study supports the notion of progressive atrial conduction disturbances with the progression of ARVC.

5 α -Dihydrotestosterone exposure interacts with plakoglobin deficiency, leading to atrial electrical dysfunction

Although commonly performed in doping, systematic observation of androgen level elevation is difficult because it is not often disclosed. Owing to the secretive or amateur nature of external AAS doping, doses and

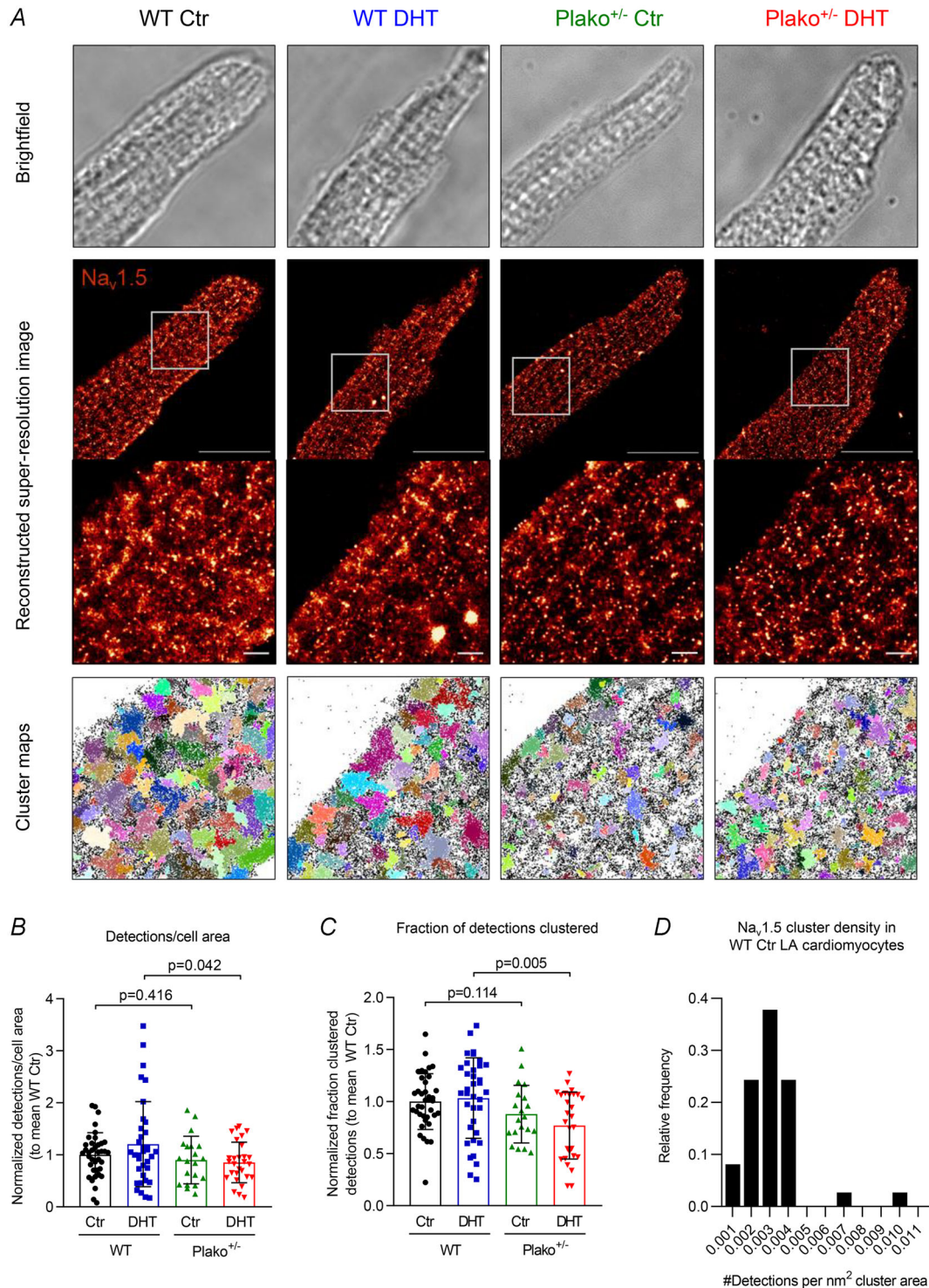


Figure 8. Sodium channel clusters in left atrial cardiomyocytes

A, brightfield images of fixed atrial cardiomyocytes before dSTORM recording (top row), reconstructed super-resolution images of membrane Na_v1.5 and high-magnification views of the indicated area (middle row), with corresponding cluster maps generated from binary images (bottom row). Detections allocated to a cluster appear in (arbitrary) colour; non-clustered detections remain black. Scale bars are 20 μ m, and 1.5 μ m for high-magnification images, respectively. B and C, genotype have a significant effect on the number of Na_v1.5 detections at the atrial cardiomyocyte membrane (B) and the fraction of Na_v1.5 detections allocated to a cluster

(C) (two-way ANOVA, $P < 0.05$). Both the number and fraction of clustered membrane $\text{Na}_v1.5$ are significantly reduced in cardiomyocytes from $\text{Plako}^{+/-}$ DHT. Results from *post hoc* Student's unpaired *t* tests are reported on the graphs. For *B* and *C*, WT Ctr, $n = 38$ cells, $N = 7$ atria; WT DHT, $n = 35/36$ cells, $N = 11$ atria; $\text{Plako}^{+/-}$ Ctr, $n = 20$ cells, $N = 5$ atria; and $\text{Plako}^{+/-}$ DHT, $n = 28$ cells, $N = 6$ atria. Data points were normalized to the mean of the respective WT Ctr group in the same imaging session. *D*, relative frequency of $\text{Na}_v1.5$ cluster densities [number of detections per naonometre squared cluster area in WT Ctr LA cardiomyocytes ($n = 38$ cells, $N = 7$ LA)]. Abbreviations: Ctr, control; DHT, 5 α -dihydrotestosterone; dSTORM, direct stochastic optical reconstruction microscopy; LA, left atrium; WT, wildtype.

plasma concentrations in humans are often unknown, but are thought to be several orders of magnitude higher than physiological levels (Vanberg & Atar, 2010). Within putatively physiological levels, Akdis et al. (2017) reported the mean total testosterone levels in male ARVC patients with adverse events to be approximately twice as high compared with ARVC patients with a favourable outcome (20 vs. 10 nmol/L, respectively).

Murine models represent a unique tool to study molecular mechanisms of elevated androgen levels in desmosomal vulnerability, including early stages of the disease, i.e. even before a clinical phenotype manifests.

We show that chronic DHT exposure prolongs the PR interval and P wave duration and slows conduction in the murine $\text{Plako}^{+/-}$ atria. Conduction slowing is a common feature of heart rhythm disorders, including AF, by permitting both micro and macro re-entry (Kirchhof, 2017).

Given that no reduction in connexin expression could be observed here, conduction slowing caused by DHT was probably mediated by locally reduced availability of sodium channels. A key determinant of conduction velocity is the magnitude of depolarizing

current, primarily carried by Na^+ through $\text{Na}_v1.5$ channels (Heijman et al., 2018). The reduction in the atrial action potential amplitude and $\text{dV}/\text{dt}_{\text{max}}$ suggests that the decrease in sodium current is sufficient to lower both the magnitude and rate of depolarization, key contributors to cardiac conduction velocity. A delay of sodium current recovery times, as observed in $\text{Plako}^{+/-}$ DHT-treated cardiomyocytes, becomes more physiologically relevant at higher pacing frequencies. The reduced availability of $\text{Na}_v1.5$ channels in cells already operating without a sufficient ‘conduction reserve’ (van Rijen et al., 2005; van Rijen & de Bakker, 2007) is likely to cause more pronounced conduction slowing and beat-to-beat variability, as observed at the higher pacing frequencies in our experiments.

5 α -Dihydrotestosterone exposure elicits subtle hypertrophy in atria

Although this is the first study showing the molecular effect on atria, it has been demonstrated previously that androgens, including DHT, induce a hypertrophic response in ventricular cardiomyocytes (Marsh et al.,

Table 3. Male sex and prevalence of atrial fibrillation (atrial arrhythmia) in arrhythmogenic right ventricular cardiomyopathy patients					
Study	Number of patients	Age [years; mean \pm SD (range)]	Male sex (%)	AA prevalence (%)	Patients with AA; male (%)
Tonet et al. (1991)	72	38 (16–73)	76	24	n.r.
Jaoude et al. (1996)	74	37.2 \pm 13.5 (11–68)	85	4	n.r.
Brembilla-Perrot et al. (1998)	47	44 \pm 18 (17–72)	70	17	63
Peters et al. (2004)	80	45.9 (22–91)	56	30	n.r.
Chu et al. (2010)	36	47 (17–80)	78	42	80
Camm et al. (2013)	248	41.6 \pm 14	53	14	69
Saguner et al. (2014)	90	49.7 \pm 14.6	63	20	61
Wu et al. (2016)	294	37.7 \pm 14.8	75	13	62
Bourfiss et al. (2016)	66	46.4 \pm 15.8	58	21	79
Mazzanti et al. (2016)	301	38 \pm 18	58	4	n.r.
Gilljam et al. (2018)	183	Median 46 (14–65)	67	9	n.r.
Wu et al. (2018)	100	37.1 \pm 12.1	78	9	n.r.
Mussigbrodt et al. (2018)	70	53.2 \pm 14.0	69	37	62
Cardona-Guarache et al. (2019)	117	52 \pm 14	60	22	69
Kikuchi et al. (2020)	90	44 \pm 15	77	36	78
Baturova et al. (2021)	100	41 (30–55)	66	28	n.r.
	Σ	Range of means:	Weighted mean:		
	1968	37.1–53.2 years	66	16	

Abbreviations: AA, atrial arrhythmia; n.r., not reported.

1998). One of the genes consistently elevated in atrial expression after DHT exposure was insulin growth factor 1 (*Igf1*), a known driver of (cardiac) muscle growth (Kim et al., 2008; Weeks et al., 2017). *Igf1* mRNA expression was also found to contribute to atrial fibrotic remodelling and AF inducibility in a rodent model (Wang et al., 2019). *IGF1*, containing an androgen response element within its promoter region (Wu et al., 2007), is a well-established target of androgen receptor-mediated gene activation. To our knowledge, we are the first to show that a supraphysiological plasma DHT concentration can induce upregulation of *Igf1* transcript levels in atria. Further evidence of the pro-hypertrophic atrial gene response to DHT exposure can be based on the downregulation of the lncRNA myosin heavy chain-associated RNA transcript (*Mhrt*). Repression of *Mhrt* expression has previously been established as a prerequisite for stress-induced, pathological cardiac hypertrophy, and restoration of *Mhrt* expression levels protected murine hearts from pressure overload-induced hypertrophy (Han et al., 2014). *Mhrt* has been shown to inhibit expression of the transcription factor myocardin (*Myocd*) (Luo et al., 2018), and increased *Myocd* expression in peripheral blood cells of patients has been associated with increased ventricular mass (Kontaraki et al., 2007). In accordance with this, downregulation of *Mhrt* expression upon DHT exposure was paralleled by upregulation of *Myocd* expression compared with control groups. Given that there was no significant increase in atrial cell diameter in histology at the investigated time point but increased cell capacitance in atrial cardiomyocytes, atrial area dilatation and increased atrial gravimetry, we propose that the atrial hypertrophic growth response to DHT seen is of an eccentric nature.

Our study demonstrates that the combination of a pro-hypertrophic, pro-inflammatory and pro-fibrotic environment caused by DHT combined with the selective reduction in I_{Na} in Plako^{+/-} cardiomyocytes is sufficient to induce conduction slowing and increased beat-to-beat heterogeneity in these vulnerable atria.

Reduced plakoglobin decreases atrial Na_v1.5 cluster availability at the membrane in response to pro-hypertrophic DHT exposure

Super-resolution imaging and electrophysiological techniques suggest that Na_v1.5 spatial sarcolemmal localization is not random but rather characterized by formation of distinct clusters (Bhargava et al., 2013; Leo-Macias et al., 2016). To our knowledge, this is the first study to evaluate the molecular arrangement of sarcolemma-localized Na_v1.5 channels in atria through the use of dSTORM to allow for visualization at nanometre resolution (localization accuracy estimated to be within 20–30 nm). The values we can estimate for

next-neighbour distance, calculated from cluster density in WT cells, are slightly lower than those reported using similar super-resolution methods in ventricular cardiac myocytes (Leo-Macias et al., 2016), suggesting slightly higher cluster densities in atrial cardiomyocytes.

The number of plasma membrane-localized Na_v1.5 detections was reduced in atrial cardiomyocytes obtained from Plako^{+/-} DHT and showed a similar trend in Plako^{+/-} control. This implies that the reduced I_{Na} density following DHT exposure in Plako^{+/-} left atria was attributable to a reduced number of membrane Na_v1.5 channels and/or defective cluster availability.

A link between plakoglobin and Na_v1.5 channel incorporation/trafficking into the cell membrane at the intercalated disc has been reported in ventricles (Asimaki et al., 2014; Noorman et al., 2013). Interactions of desmosomal and intercalated disc proteins with the sodium channel complex have been demonstrated in ventricles previously (Rizzo et al., 2012), and loss or mutations of the desmosomal components plakophilin-2 and desmoglein-2 were associated with reduced cardiac (ventricular) sodium current in different cell and murine models (Cerrone et al., 2014; Rizzo et al., 2012; Sato et al., 2009).

Although this report is the first to demonstrate altered sodium channel expression upon androgenic steroid challenge in cardiomyocytes, steroid hormones have known effects on neuronal sodium channel expression (Borner et al., 2006), and androgenic steroids have non-genomic effects on calcium signalling (Vicencio et al., 2011). Our key finding of altered sodium channel clustering suggests a direct involvement of vulnerable desmosomes rather than a genomic effect of androgenic steroids. Future studies might determine whether the altered sodium channel clustering is attributable to a non-genomic direct effect of DHT or to an increased vulnerability to increased volume load and hypertrophic stimuli induced by steroid exposure.

A mismatch in cell size caused by hypertrophic stimuli, such as androgenic steroid exposure, and Na_v1.5 cluster availability could have implications for other cardiomyopathies and forms of pathological hypertrophy (Hofmann et al., 2012; Wagner et al., 2006). The understanding of the role of ion channel subcellular localization, especially cluster properties, is in its infancy (Marchal & Remme, 2022), but our observations are consistent with other recent studies reporting a reduced I_{Na} in response to changes in single-molecule Na_v1.5 organization (Agullo-Pascual et al., 2014; te Riele et al., 2017).

Limitations

Although we show a reduction in Na_v1.5 function (I_{Na}) and in Na_v1.5 clustering at the membrane when

plakoglobin deficiency and AAS are combined, the factors directly linking them and other desmosomal proteins deserve further study. We targeted the sodium channel because this was most promising regarding the functional changes seen. The effects of AAS on calcium handling will be worth exploring, particularly in ARVC models with an established disturbance in calcium signalling (Kim, Perez-Hernandez, et al., 2019; van Opbergen et al., 2019).

Androgenic anabolic steroid users are more likely to participate in high levels of exercise. These might enhance or reverse the effects of androgenic steroids. Although metabolic effects of DHT on, for example, lipids could be reversed, in part, by exercise, effects on cardiac electrophysiology are likely to be multiplied, taking into account that high levels of exercise have been shown to lead to earlier manifestation and disease progression in ARVC (James et al., 2013; Kirchhof et al., 2006) and AF (Benito et al., 2011; Guasch et al., 2013). A wide variety of anabolic steroid substances are commonly used by athletes, and some might have different effects on the pathways studied here.

In the patients and in the murine models studied, left ventricular function was sustained. We cannot rule out atrial remodelling secondary to left ventricular hypertrophy in the AAS-exposed mice with plakoglobin deficiency.

Only a small proportion of ARVC patients carry plakoglobin variants, and studies in other models should be performed. The Plako^{+/-} model was chosen because it causes an ARVC phenotype but lacks ventricular remodelling at the age studied here, enabling the study of atrial effects without interference by ventricular dysfunction or heart failure. Additionally, plakoglobin reduction is found in hearts of patients with ARVC carrying different mutations (Asimaki et al., 2009) and can therefore be considered as a common pathway contributing to ARVC.

References

- Ackers-Johnson, M., Li, P. Y., Holmes, A. P., O'Brien, S. M., Pavlovic, D., & Foo, R. S. (2016). A simplified, Langendorff-free method for concomitant isolation of viable cardiac myocytes and non-myocytes from the adult mouse heart. *Circulation Research*, **119**(8), 909–920.
- Agullo-Pascual, E., Lin, X. M., Leo-Macias, A., Zhang, M. L., Liang, F. X., Li, Z., Pfenniger, A., Lubkemeier, I., Keegan, S., Fenyó, D., Willecke, K., Rothenberg, E., & Delmar, M. (2014). Super-resolution imaging reveals that loss of the C-terminus of connexin43 limits microtubule plus-end capture and Na(V)1.5 localization at the intercalated disc. *Cardiovascular Research*, **104**(2), 371–381.
- Akcakoyun, M., Alizade, E., Gundogdu, R., Bulut, M., Tabakci, M. M., Acar, G., Avci, A., Simsek, Z., Fidan, S., Demir, S., Kargin, R., & Emiroglu, M. Y. (2014). Long-term anabolic androgenic steroid use is associated with increased atrial electromechanical delay in male bodybuilders. *BioMed Research International*, **2014**, 451520.
- Akdis, D., Saguner, A. M., Shah, K., Wei, C., Medeiros-Domingo, A., von Eckardstein, A., Luscher, T. F., Brunckhorst, C., Chen, H. S., & Duru, F. (2017). Sex hormones affect outcome in arrhythmogenic right ventricular cardiomyopathy/dysplasia: From a stem cell derived cardiomyocyte-based model to clinical biomarkers of disease outcome. *European Heart Journal*, **38**(19), 1498–1508.
- Alizade, E., Avci, A., Fidan, S., Tabakci, M., Bulut, M., Zehir, R., Simsek, Z., Evlice, M., Arslantas, U., Cakir, H., Emiroglu, M. Y., & Akcakoyun, M. (2015). The effect of chronic anabolic-androgenic steroid use on Tp-E interval, Tp-E/Qt ratio, and Tp-E/Qt ratio in male bodybuilders. *Annals of Noninvasive Electrocardiology*, **20**(6), 592–600.
- Aljehani, A., Kew, T., Baig, S., Cox, H., Sommerfeld, L. C., Ensam, B., Kalla, M., Steeds, R. P., & Fabritz, L. (2023). Characterisation of patients referred to a tertiary-level inherited cardiac condition clinic with suspected arrhythmogenic right ventricular cardiomyopathy (ARVC). *BMC Cardiovascular Disorders [Electronic Resource]*, **23**(1), 14.
- Anders, S., Pyl, P. T., & Huber, W. (2015). HTSeq—a Python framework to work with high-throughput sequencing data. *Bioinformatics (Oxford, England)*, **31**(2), 166–169.
- Antoniades, L., Tsatsopoulou, A., Anastakis, A., Syrris, P., Asimaki, A., Panagiotakos, D., Zambartas, C., Stefanadis, C., McKenna, W. J., & Protonotarios, N. (2006). Arrhythmogenic right ventricular cardiomyopathy caused by deletions in plakophilin-2 and plakoglobin (Naxos disease) in families from Greece and Cyprus: Genotype-phenotype relations, diagnostic features and prognosis. *European Heart Journal*, **27**(18), 2208–2216.
- Asimaki, A., Kapoor, S., Plovie, E., Arndt, A. K., Adams, E., Liu, Z. Z., James, C. A., Judge, D. P., Calkins, H., Churko, J., Wu, J. C., MacRae, C. A., Kleber, A. G., & Saffitz, J. E. (2014). Identification of a new modulator of the intercalated disc in a zebrafish model of arrhythmogenic cardiomyopathy. *Science Translational Medicine*, **6**(240), 240ra74.
- Asimaki, A., Syrris, P., Wichter, T., Matthias, P., Saffitz, J. E., & McKenna, W. J. (2007). A novel dominant mutation in plakoglobin causes Arrhythmogenic right ventricular cardiomyopathy. *American Journal of Human Genetics*, **81**(5), 964–973.
- Asimaki, A., Tandri, H., Huang, H., Halushka, M. K., Gautam, S., Basso, C., Thiene, G., Tsatsopoulou, A., Protonotarios, N., McKenna, W. J., Calkins, H., & Saffitz, J. E. (2009). A new diagnostic test for arrhythmogenic right ventricular cardiomyopathy. *New England Journal of Medicine*, **360**(11), 1075–1084.
- Baturova, M. A., Haugaa, K. H., Jensen, H. K., Svensson, A., Gilljam, T., Bundgaard, H., Madsen, T., Hansen, J., Chivulescu, M., Christiansen, M. K., Carlson, J., Edvardsen, T., Svendsen, J. H., & Platonov, P. G. (2020). Atrial fibrillation as a clinical characteristic of arrhythmogenic right ventricular cardiomyopathy: Experience from the Nordic ARVC Registry. *International Journal of Cardiology*, **298**, 39–43.

- Baturova, M. A., Svensson, A., Aneq, M. A., Svendsen, J. H., Risum, N., Sherina, V., Bundgaard, H., Meurling, C., Lundin, C., Carlson, J., & Platonov, P. G. (2021). Evolution of P-wave indices during long-term follow-up as markers of atrial substrate progression in arrhythmogenic right ventricular cardiomyopathy. *Europace : European Pacing, Arrhythmias, and Cardiac Electrophysiology : Journal of the Working Groups on Cardiac Pacing, Arrhythmias, and Cardiac Cellular Electrophysiology of the European Society of Cardiology*, **23**, (23 Suppl 1), i29–i37.
- Benito, B., Gay-Jordi, G., Serrano-Mollar, A., Guasch, E., Shi, Y., Tardif, J. C., Brugada, J., Nattel, S., & Mont, L. (2011). Cardiac arrhythmogenic remodeling in a rat model of long-term intensive exercise training. *Circulation*, **123**(1), 13–22.
- Berger, D., Folsom, A. R., Schreiner, P. J., Chen, L. Y., Michos, E. D., O'Neal, W. T., Soliman, E. Z., & Alonso, A. (2019). Plasma total testosterone and risk of incident atrial fibrillation: The Atherosclerosis Risk in Communities (ARIC) study. *Maturitas*, **125**, 5–10.
- Bhargava, A., Lin, X. M., Novak, P., Mehta, K., Korchev, Y., Delmar, M., & Gorelik, J. (2013). Super-resolution scanning patch clamp reveals clustering of functional ion channels in adult ventricular myocyte. *Circulation Research*, **112**(8), 1112–1120.
- Borner, J., Puschmann, T., & Duch, C. (2006). A steroid hormone affects sodium channel expression in *Manduca* central neurons. *Cell and Tissue Research*, **325**(1), 175–187.
- Bourfiss, M., Te Riele, A. S., Mast, T. P., Cramer, M. J., JF, V. D. H., TA, V., Loh, P., Dooijes, D., Hauer, R. N., & Velthuis, B. K. (2016). Influence of genotype on structural atrial abnormalities and atrial fibrillation or flutter in arrhythmogenic right ventricular dysplasia/cardiomyopathy. *Journal of Cardiovascular Electrophysiology*, **27**(12), 1420–1428.
- Brembilla-Perrot, B., Jacquemin, L., Houplon, P., Houriez, P., Beurrier, D., Berder, V., Terrier de la Chaise, A., & Louis, P. (1998). Increased atrial vulnerability in arrhythmogenic right ventricular disease. *American Heart Journal*, **135**(5 Pt 1), 748–754.
- Camm, C. F., James, C. A., Tichnell, C., Murray, B., Bhonsale, A., te Riele, A. S., Judge, D. P., Tandri, H., & Calkins, H. (2013). Prevalence of atrial arrhythmias in arrhythmogenic right ventricular dysplasia/cardiomyopathy. *Heart Rhythm*, **10**(11), 1661–1668.
- Cardona-Guarache, R., Astrom-Aneq, M., Oesterle, A., Asirvatham, R., Svetlichnaya, J., Marcus, G. M., Gerstenfeld, E. P., Klein, L., & Scheinman, M. M. (2019). Atrial arrhythmias in patients with arrhythmogenic right ventricular cardiomyopathy: Prevalence, echocardiographic predictors, and treatment. *Journal of Cardiovascular Electrophysiology*, **30**(10), 1801–1810.
- Cerrone, M., Lin, X., Zhang, M., Agullo-Pascual, E., Pfenniger, A., Chkourko Gusk, H., Novelli, V., Kim, C., Tirasawadichai, T., Judge, D. P., Rothenberg, E., Chen, H. S., Napolitano, C., Priori, S. G., & Delmar, M. (2014). Missense mutations in plakophilin-2 cause sodium current deficit and associate with a Brugada syndrome phenotype. *Circulation*, **129**(10), 1092–1103.
- Chu, A. F., Zado, E., & Marchlinski, F. E. (2010). Atrial arrhythmias in patients with arrhythmogenic right ventricular cardiomyopathy/dysplasia and ventricular tachycardia. *The American Journal of Cardiology*, **106**(5), 720–722.
- Fabritz, L., Hoogendijk, M. G., Scicluna, B. P., van Amersfoort, S. C., Fortmueller, L., Wolf, S., Laakmann, S., Kreienkamp, N., Piccini, I., Breithardt, G., Noppinger, P. R., Witt, H., Ebnet, K., Wichter, T., Levkau, B., Franke, W. W., Pieperhoff, S., de Bakker, J. M., Coronel, R., & Kirchhof, P. (2011). Load-reducing therapy prevents development of arrhythmogenic right ventricular cardiomyopathy in plakoglobin-deficient mice. *Journal of the American College of Cardiology*, **57**(6), 740–750.
- Fineschi, V., Riezzo, I., Centini, F., Silingardi, E., Licata, M., Beduschi, G., & Karch, S. B. (2007). Sudden cardiac death during anabolic steroid abuse: Morphologic and toxicologic findings in two fatal cases of bodybuilders. *International Journal of Legal Medicine*, **121**(1), 48–53.
- Furlanello, F., Serdoz, L. V., Cappato, R., & De Ambroggi, L. (2007). Illicit drugs and cardiac arrhythmias in athletes. *European Journal of Cardiovascular Prevention and Rehabilitation*, **14**(4), 487–494.
- Gasperetti, A., James, C. A., Chen, L., Schenker, N., Casella, M., Kany, S., Mathew, S., Compagnucci, P., Mussigbrodt, A., Jensen, H. K., Svensson, A., Costa, S., Forleo, G. B., Platonov, P. G., Tondo, C., Song, J. P., Dello Russo, A., Ruschitzka, F., Brunckhorst, C., ... Saguner, A. M. (2021). Efficacy of catheter ablation for atrial arrhythmias in patients with arrhythmogenic right ventricular cardiomyopathy—a multicenter study. *Journal of Clinical Medicine*, **10**(21), 4962.
- Gilljam, T., Haugaa, K. H., Jensen, H. K., Svensson, A., Bundgaard, H., Hansen, J., Dellgren, G., Gustafsson, F., Eiskjaer, H., Andreassen, A. K., Sjogren, J., Edvardsen, T., Holst, A. G., Svendsen, J. H., & Platonov, P. G. (2018). Heart transplantation in arrhythmogenic right ventricular cardiomyopathy - Experience from the Nordic ARVC Registry. *International Journal of Cardiology*, **250**, 201–206.
- Gorenk, B., Birdane, A., Kudaiberdieva, G., Goktekin, O., Cavusoglu, Y., Unalir, A., Ata, N., & Timuralp, B. (2003). P wave amplitude and duration may predict immediate recurrence of atrial fibrillation after internal cardioversion. *Annals of Noninvasive Electrocardiology*, **8**(3), 215–218.
- Guasch, E., Benito, B., Qi, X., Cifelli, C., Naud, P., Shi, Y., Mighiu, A., Tardif, J. C., Tadevosyan, A., Chen, Y., Gillis, M. A., Iwasaki, Y. K., Dobrev, D., Mont, L., Heximer, S., & Nattel, S. (2013). Atrial fibrillation promotion by endurance exercise: Demonstration and mechanistic exploration in an animal model. *Journal of the American College of Cardiology*, **62**(1), 68–77.
- Han, P., Li, W., Lin, C. H., Yang, J., Shang, C., Nuernberg, S. T., Jin, K. K., Xu, W., Lin, C. Y., Lin, C. J., Xiong, Y., Chien, H., Zhou, B., Ashley, E., Bernstein, D., Chen, P. S., Chen, H. V., Quertermous, T., & Chang, C. P. (2014). A long noncoding RNA protects the heart from pathological hypertrophy. *Nature*, **514**(7520), 102–106.

- Heijman, J., Guichard, J. B., Dobrev, D., & Nattel, S. (2018). Translational challenges in atrial fibrillation. *Circulation Research*, **122**(5), 752–773.
- Hofmann, F., Fabritz, L., Stieber, J., Schmitt, J., Kirchhof, P., Ludwig, A., & Herrmann, S. (2012). Ventricular HCN channels decrease the repolarization reserve in the hypertrophic heart. *Cardiovascular Research*, **95**(3), 317–326.
- Holmes, A. P., Yu, T. Y., Tull, S., Syeda, F., Kuhlmann, S. M., O'Brien, S.-M., Patel, P., Brain, K. L., Pavlovic, D., Brown, N. A., Fabritz, L., & Kirchhof, P. (2016). A regional reduction in ito and IKACH in the murine posterior left atrial myocardium is associated with action potential prolongation and increased ectopic activity. *PLoS ONE*, **11**(5), e0154077.
- James, C. A., Bhonsale, A., Tichnell, C., Murray, B., Russell, S. D., Tandri, H., Tedford, R. J., Judge, D. P., & Calkins, H. (2013). Exercise increases age-related penetrance and arrhythmic risk in arrhythmogenic right ventricular dysplasia/cardiomyopathy-associated desmosomal mutation carriers. *Journal of the American College of Cardiology*, **62**(14), 1290–1297.
- Jaoude, S. A., Leclercq, J. F., & Coumel, P. (1996). Progressive ECG changes in arrhythmogenic right ventricular disease. Evidence for an evolving disease. *European Heart Journal*, **17**(11), 1717–1722.
- Kikuchi, N., Shiga, T., Suzuki, A., & Hagiwara, N. (2020). Atrial tachyarrhythmias and heart failure events in patients with arrhythmogenic right ventricular cardiomyopathy. *International Journal of Cardiology-Heart & Vasculture*, **31**, 100669.
- Kim, D., Paggi, J. M., Park, C., Bennett, C., & Salzberg, S. L. (2019). Graph-based genome alignment and genotyping with HISAT2 and HISAT-genotype. *Nature Biotechnology*, **37**(8), 907–915.
- Kim, J., Wende, A. R., Sena, S., Theobald, H. A., Soto, J., Sloan, C., Wayment, B. E., Litwin, S. E., Holzenberger, M., LeRoith, D., & Abel, E. D. (2008). Insulin-like growth factor I receptor signaling is required for exercise-induced cardiac hypertrophy. *Molecular Endocrinology*, **22**(11), 2531–2543.
- Kim, J. C., Perez-Hernandez, M., Alvarado, F. J., Maurya, S. R., Montnach, J., Yin, Y., Zhang, M., Lin, X., Vasquez, C., Heguy, A., Liang, F. X., Woo, S. H., Morley, G. E., Rothenberg, E., Lundby, A., Valdivia, H. H., Cerrone, M., & Delmar, M. (2019). Disruption of Ca(2+) homeostasis and connexin 43 hemichannel function in the right ventricle precedes overt arrhythmogenic cardiomyopathy in Plakophilin-2-Deficient mice. *Circulation*, **140**(12), 1015–1030.
- Kirchhof, P. (2017). The future of atrial fibrillation management: Integrated care and stratified therapy. *Lancet*, **390**(10105), 1873–1887.
- Kirchhof, P., Fabritz, L., Zwiener, M., Witt, H., Schafers, M., Zellerhoff, S., Paul, M., Athai, T., Hiller, K. H., Baba, H. A., Breithardt, G., Ruiz, P., Wichter, T., & Levkau, B. (2006). Age- and training-dependent development of arrhythmogenic right ventricular cardiomyopathy in heterozygous plakoglobin-deficient mice. *Circulation*, **114**(17), 1799–1806.
- Kirchhof, P., Kahr, P. C., Kaese, S., Piccini, I., Vokshi, I., Scheld, H. H., Rotering, H., Fortmueller, L., Laakmann, S., Verheule, S., Schotten, U., Fabritz, L., & Brown, N. A. (2011). PITX2c is expressed in the adult left atrium, and reducing Pitx2c expression promotes atrial fibrillation inducibility and complex changes in gene expression. *Circulation Cardiovascular Genetics*, **4**(2), 123–133.
- Kontarakis, J. E., Parthenakis, F. I., Patrianakos, A. P., Karalis, I. K., & Vardas, P. E. (2007). Altered expression of early cardiac marker genes in circulating cells of patients with hypertrophic cardiomyopathy. *Cardiovascular Pathology*, **16**(6), 329–335.
- Kulle, A. E., Riepe, F. G., Melchior, D., Hiort, O., & Holterhus, P. M. (2010). A novel ultrahigh-pressure liquid chromatography tandem mass spectrometry method for the simultaneous determination of androstenedione, testosterone, and dihydrotestosterone in pediatric blood samples: Age- and sex-specific reference data. *Journal of Clinical Endocrinology and Metabolism*, **95**(5), 2399–2409.
- Lau, D. H., Stiles, M. K., John, B., Shashidhar, Young, G. D., & Sanders, P. (2007). Atrial fibrillation and anabolic steroid abuse. *International Journal of Cardiology*, **117**(2), e86–e87.
- Leo-Macias, A., Agullo-Pascual, E., Sanchez-Alonso, J. L., Keegan, S., Lin, X. M., Arcos, T., Feng Xia, L., Korchev, Y. E., Gorelik, J., Fenyo, D., Rothenberg, E., & Delmar, M. (2016). Nanoscale visualization of functional adhesion/excitability nodes at the intercalated disc. *Nature Communications*, **7**, 10342.
- Li, H., Handsaker, B., Wysoker, A., Fennell, T., Ruan, J., Homer, N., Marth, G., Abecasis, G., Durbin, R., & Genome Project Data Processing S. (2009). The sequence alignment/map format and SAMtools. *Bioinformatics (Oxford, England)*, **25**(16), 2078–2079.
- Li, J., Swope, D., Raess, N., Cheng, L., Muller, E. J., & Radice, G. L. (2011). Cardiac tissue-restricted deletion of plakoglobin results in progressive cardiomyopathy and activation of {beta}-catenin signaling. *Molecular and Cellular Biology*, **31**(6), 1134–1144.
- Love, M. I., Huber, W., & Anders, S. (2014). Moderated estimation of fold change and dispersion for RNA-seq data with DESeq2. *Genome Biology*, **15**(12), 550.
- Luijckx, T., Velthuis, B. K., Backx, F. J. G., Buckens, C. F. M., Prakken, N. H. J., Rienks, R., Mali, W., & Cramer, M. J. (2013). Anabolic androgenic steroid use is associated with ventricular dysfunction on cardiac MRI in strength trained athletes. *International Journal of Cardiology*, **167**(3), 664–668.
- Luo, Y., Xu, Y., Liang, C., Xing, W., & Zhang, T. (2018). The mechanism of myocardial hypertrophy regulated by the interaction between mHrt and myocardin. *Cell. Signalling*, **43**, 11–20.
- Magnani, J. W., Zhu, L., Lopez, F., Pencina, M. J., Agarwal, S. K., Soliman, E. Z., Benjamin, E. J., & Alonso, A. (2015). P-wave indices and atrial fibrillation: Cross-cohort assessments from the Framingham Heart Study (FHS) and Atherosclerosis Risk in Communities (ARIC) study. *American Heart Journal*, **169**(1), 53–61.e1.
- Marchal, G. A., & Remme, C. A. (2022). Subcellular diversity of Nav1.5 in cardiomyocytes: Distinct functions, mechanisms and targets. *The Journal of Physiology*, **601**(5), 941–960.

- Marcus, F. I., McKenna, W. J., Sherrill, D., Basso, C., Bauce, B., Bluemke, D. A., Calkins, H., Corrado, D., Cox, M. G., Daubert, J. P., Fontaine, G., Gear, K., Hauer, R., Nava, A., Picard, M. H., Protonotarios, N., Saffitz, J. E., Sanborn, D. M., Steinberg, J. S., ... Zareba, W. (2010). Diagnosis of arrhythmogenic right ventricular cardiomyopathy/dysplasia: Proposed modification of the Task Force Criteria. *European Heart Journal*, **31**(7), 806–814.
- Marsh, J. D., Lehmann, M. H., Ritchie, R. H., Gwathmey, J. K., Green, G. E., & Schiebinger, R. J. (1998). Androgen receptors mediate hypertrophy in cardiac myocytes. *Circulation*, **98**(3), 256–261.
- Mazzanti, A., Ng, K., Faragli, A., Maragna, R., Chiodaroli, E., Orphanou, N., Monteforte, N., Memmi, M., Gambelli, P., Novelli, V., Bloise, R., Catalano, O., Moro, G., Tibollo, V., Morini, M., Bellazzi, R., Napolitano, C., Bagnardi, V., & Priori, S. G. (2016). Arrhythmogenic right ventricular cardiomyopathy: Clinical course and predictors of arrhythmic risk. *Journal of the American College of Cardiology*, **68**(23), 2540–2550.
- McKoy, G., Protonotarios, N., Crosby, A., Tsatsopoulou, A., Anastasakis, A., Coonar, A., Norman, M., Baboonian, C., Jeffery, S., & McKenna, W. J. (2000). Identification of a deletion in plakoglobin in arrhythmogenic right ventricular cardiomyopathy with palmoplantar keratoderma and woolly hair (Naxos disease). *Lancet (London, England)*, **355**(9221), 2119–2124.
- Medei, E., Marocolo, M., Rodrigues, D. D., Arantes, P. C., Takiya, C. M., Silva, J., Rondinelli, E., Goldenberg, R. C. D., de Carvalho, A. C. C., & Nascimento, J. H. M. (2010). Chronic treatment with anabolic steroids induces ventricular repolarization disturbances: Cellular, ionic and molecular mechanism. *Journal of Molecular and Cellular Cardiology*, **49**(2), 165–175.
- Morita, H., Kusano-Fukushima, K., Nagase, S., Fujimoto, Y., Hisamatsu, K., Fujio, H., Haraoka, K., Kobayashi, M., Morita, S. T., Nakamura, K., Emori, T., Matsubara, H., Hina, K., Kita, T., Fukatani, M., & Ohe, T. (2002). Atrial fibrillation and atrial vulnerability in patients with Brugada syndrome. *Journal of the American College of Cardiology*, **40**(8), 1437–1444.
- Mussigbrodt, A., Knopp, H., Efimova, E., Weber, A., Bertagnolli, L., Hilbert, S., Kosiuk, J., Dinov, B., Bode, K., Kircher, S., Dagres, N., Richter, S., Sommer, P., Husser, D., Bollmann, A., Hindricks, G., & Arya, A. (2018). Supra-ventricular arrhythmias in patients with arrhythmogenic right ventricular dysplasia/cardiomyopathy associate with long-term outcome after catheter ablation of ventricular tachycardias. *Europace : European pacing, Arrhythmias, and Cardiac Electrophysiology : Journal of the Working Groups on Cardiac Pacing, Arrhythmias, and Cardiac Cellular Electrophysiology of the European Society of Cardiology*, **20**(7), 1182–1187.
- Nieschlag, E., & Vorona, E. (2015). Doping with anabolic androgenic steroids (AAS): Adverse effects on non-reproductive organs and functions. *Reviews in Endocrine & Metabolic Disorders*, **16**(3), 199–211.
- Noorman, M., Hakim, S., Kessler, E., Groeneweg, J. A., Cox, M., Asimaki, A., van Rijen, H. V. M., van Stuijvenberg, L., Chkourko, H., van der Heyden, M. A. G., Vos, M. A., de Jonge, N., van der Smagt, J. J., Dooijes, D., Vink, A., de Weger, R. A., Varro, A., de Bakker, J. M. T., Saffitz, J. E., ... van Veen, T. A. B. (2013). Remodeling of the cardiac sodium channel, connexin43, and plakoglobin at the intercalated disk in patients with arrhythmogenic cardiomyopathy. *Heart Rhythm : The Official Journal of the Heart Rhythm Society*, **10**(3), 412–419.
- O'Shea, C., Holmes, A. P., Yu, T. Y., Winter, J., Wells, S. P., Correia, J., Boukens, B. J., De Groot, J. R., Chu, G. S., Li, X., Ng, G. A., Kirchhof, P., Fabritz, L., Rajpoot, K., & Pavlovic, D. (2019). ElectroMap: High-throughput open-source software for analysis and mapping of cardiac electrophysiology. *Scientific Reports*, **9**(1), 1389.
- Obergassel, J., O'Reilly, M., Sommerfeld, L. C., Kabir, S. N., O'Shea, C., Syeda, F., Eckardt, L., Kirchhof, P., & Fabritz, L. (2021). Effects of genetic background, sex, and age on murine atrial electrophysiology. *Europace : European Pacing, Arrhythmias, and Cardiac Electrophysiology : Journal of the Working Groups on Cardiac Pacing, Arrhythmias, and Cardiac Cellular Electrophysiology of the European Society of Cardiology*, **23**(6), 958–969.
- Ovesny, M., Krizek, P., Borkovec, J., Svindrych, Z., & Hagen, G. M. (2014). ThunderSTORM: A comprehensive ImageJ plug-in for PALM and STORM data analysis and super-resolution imaging. *Bioinformatics (Oxford, England)*, **30**(16), 2389–2390.
- Peters, S., Trummel, M., & Meyners, W. (2004). Prevalence of right ventricular dysplasia-cardiomyopathy in a non-referral hospital. *International Journal of Cardiology*, **97**(3), 499–501.
- Pike, J. A., Khan, A. O., Pallini, C., Thomas, S. G., Mund, M., Ries, J., Poulter, N. S., & Styles, I. B. (2020). Topological data analysis quantifies biological nano-structure from single molecule localization microscopy. *Bioinformatics (Oxford, England)*, **36**(5), 1614–1621.
- Pirompol, P., Teekabut, V., Weerachatanukul, W., Bupha-Intr, T., & Wattanapernpool, J. (2016). Supra-physiological dose of testosterone induces pathological cardiac hypertrophy. *Journal of Endocrinology*, **229**(1), 13–23.
- Platonov, P. G., Christensen, A. H., Holmqvist, F., Carlson, J., Haunso, S., & Svendsen, J. H. (2011). Abnormal atrial activation is common in patients with arrhythmogenic right ventricular cardiomyopathy. *Journal of Electrocardiology*, **44**(2), 237–241.
- Priori, S. G., Blomstrom-Lundqvist, C., Mazzanti, A., Blom, N., Borggrefe, M., Camm, J., Elliott, P. M., Fitzsimons, D., Hatala, R., Hindricks, G., Kirchhof, P., Kjeldsen, K., Kuck, K. H., Hernandez-Madrid, A., Nikolaou, N., Norekval, T. M., Spaulding, C., & Van Veldhuisen, D. J. (2015). 2015 ESC Guidelines for the management of patients with ventricular arrhythmias and the prevention of sudden cardiac death: The Task Force for the Management of Patients with Ventricular Arrhythmias and the Prevention of Sudden Cardiac Death of the European Society of Cardiology (ESC). Endorsed by: Association for European Paediatric and Congenital Cardiology (AEPC). *European Heart Journal*, **36**(41), 2793–2867.

- Protonotarios, N., Tsatsopoulou, A., Anastasakis, A., Sevdalis, E., McKoy, G., Stratos, K., Gatzoulis, K., Tentolouris, K., Spiliopoulou, C., Panagiotakos, D., McKenna, W., & Toutouzas, P. (2001). Genotype-phenotype assessment in autosomal recessive arrhythmogenic right ventricular cardiomyopathy (Naxos disease) caused by a deletion in plakoglobin. *Journal of the American College of Cardiology*, **38**(5), 1477–1484.
- Rizzo, S., Lodder, E. M., Verkerk, A. O., Wolswinkel, R., Beekman, L., Pilichou, K., Basso, C., Remme, C. A., Thiene, G., & Bezzina, C. R. (2012). Intercalated disc abnormalities, reduced Na(+) current density, and conduction slowing in desmoglein-2 mutant mice prior to cardiomyopathic changes. *Cardiovascular Research*, **95**(4), 409–418.
- Rootwelt-Norberg, C., Lie, O. H., Chivulescu, M., Castrini, A. I., Sarvari, S. I., Lyseggen, E., Almaas, V. M., Bogsrud, M. P., Edvardsen, T., & Haugaa, K. H. (2021). Sex differences in disease progression and arrhythmic risk in patients with arrhythmogenic cardiomyopathy. *Europace : European Pacing, Arrhythmias, and Cardiac Electrophysiology : Journal of the Working Groups on Cardiac Pacing, Arrhythmias, and Cardiac Cellular Electrophysiology of the European Society of Cardiology*, **23**(7), 1084–1091.
- Roselli, C., Chaffin, M. D., Weng, L. C., Aeschbacher, S., Ahlberg, G., Albert, C. M., Almgren, P., Alonso, A., Anderson, C. D., Aragam, K. G., Arking, D. E., Barnard, J., Bartz, T. M., Benjamin, E. J., Bihlmeyer, N. A., Bis, J. C., Bloom, H. L., Boerwinkle, E., Bottinger, E. B., ... Ellinor, P. T. (2018). Multi-ethnic genome-wide association study for atrial fibrillation. *Nature Genetics*, **50**(9), 1225–1233.
- Sagoe, D., Molde, H., Andreassen, C. S., Torsheim, T., & Pallesen, S. (2014). The global epidemiology of anabolic-androgenic steroid use: A meta-analysis and meta-regression analysis. *Annals of Epidemiology*, **24**(5), 383–398.
- Saguner, A. M., Ganahl, S., Kraus, A., Baldinger, S. H., Medeiros-Domingo, A., Saguner, A. R., Mueller-Burri, S. A., Wolber, T., Haegeli, L. M., Krasniqi, N., Tanner, F. C., Steffl, J., Brunnkhorst, C., & Duru, F. (2014). Clinical role of atrial arrhythmias in patients with arrhythmogenic right ventricular dysplasia. *Circulation Journal : Official Journal of the Japanese Circulation Society*, **78**(12), 2854–2861.
- Sato, P. Y., Musa, H., Coombs, W., Guerrero-Serna, G., Patino, G. A., Taffet, S. M., Isom, L. L., & Delmar, M. (2009). Loss of plakophilin-2 expression leads to decreased sodium current and slower conduction velocity in cultured cardiac myocytes. *Circulation Research*, **105**(6), 523–526.
- Soliman, E. Z., Prineas, R. J., Case, L. D., Zhang, Z. M., & Goff, D. C., Jr (2009). Ethnic distribution of ECG predictors of atrial fibrillation and its impact on understanding the ethnic distribution of ischemic stroke in the Atherosclerosis Risk in Communities (ARIC) study. *Stroke; A Journal of Cerebral Circulation*, **40**(4), 1204–1211.
- Spencer, C. I., Yuill, K. H., Borg, J. J., Hancox, J. C., & Kozlowski, R. Z. (2001). Actions of pyrethroid insecticides on sodium currents, action potentials, and contractile rhythm in isolated mammalian ventricular myocytes and perfused hearts. *Journal of Pharmacology and Experimental Therapeutics*, **298**(3), 1067–1082.
- Sullivan, M. L., Martinez, C. M., & Gallagher, E. J. (1999). Atrial fibrillation and anabolic steroids. *Journal of Emergency Medicine*, **17**(5), 851–857.
- Syeda, F., Holmes, A. P., Yu, T. Y., Tull, S., Kuhlmann, S. M., Pavlovic, D., Betney, D., Riley, G., Kucera, J. P., Jousset, F., de Groot, J. R., Rohr, S., Brown, N. A., Fabritz, L., & Kirchhof, P. (2016). PITX2 modulates atrial membrane potential and the antiarrhythmic effects of sodium-channel blockers. *Journal of the American College of Cardiology*, **68**(17), 1881–1894.
- Takehara, N., Makita, N., Kawabe, J., Sato, N., Kawamura, Y., Kitabatake, A., & Kikuchi, K. (2004). A cardiac sodium channel mutation identified in Brugada syndrome associated with atrial standstill. *Journal of Internal Medicine*, **255**(1), 137–142.
- te Riele, A., Agullo-Pascual, E., James, C. A., Leo-Macias, A., Cerrone, M., Zhang, M. L., Lin, X. M., Lin, B., Rothenberg, E., Sobreira, N. L., Amat-Alarcon, N., Marsman, R. F., Murray, B., Tichnell, C., van der Heijden, J. F., Dooijes, D., van Veen, T. A. B., Tandri, H., Fowler, S. J., ... Judge, D. P. (2017). Multilevel analyses of SCN5A mutations in arrhythmogenic right ventricular dysplasia/cardiomyopathy suggest non-canonical mechanisms for disease pathogenesis. *Cardiovascular Research*, **113**(1), 102–111.
- Tonet, J. L., Castro-Miranda, R., Iwa, T., Poulain, F., Frank, R., & Fontaine, G. H. (1991). Frequency of supraventricular tachyarrhythmias in arrhythmogenic right ventricular dysplasia. *The American Journal of Cardiology*, **67**(13), 1153.
- Tsai, W. C., Lee, T. I., Chen, Y. C., Kao, Y. H., Lu, Y. Y., Lin, Y. K., Chen, S. A., & Chen, Y. J. (2014). Testosterone replacement increases aged pulmonary vein and left atrium arrhythmogenesis with enhanced adrenergic activity. *International Journal of Cardiology*, **176**(1), 110–118.
- Urhausen, A., Albers, T., & Kindermann, W. (2004). Are the cardiac effects of anabolic steroid abuse in strength athletes reversible? *Heart*, **90**(5), 496–501.
- van Opbergen, C. J. M., Noorman, M., Pfenniger, A., Copier, J. S., Vermij, S. H., Li, Z., van der Nagel, R., Zhang, M., de Bakker, J. M. T., Glass, A. M., Mohler, P. J., Taffet, S. M., Vos, M. A., van Rijen, H. V. M., Delmar, M., & van Veen, T. A. B. (2019). Plakophilin-2 haploinsufficiency causes calcium handling deficits and modulates the cardiac response towards stress. *International Journal of Molecular Sciences*, **20**(17), 4076.
- van Rijen, H. V., & de Bakker, J. M. (2007). Penetrance of monogenetic cardiac conduction diseases. A matter of conduction reserve? *Cardiovascular Research*, **76**(3), 379–380.
- van Rijen, H. V., de Bakker, J. M., & van Veen, T. A. (2005). Hypoxia, electrical uncoupling, and conduction slowing: Role of conduction reserve. *Cardiovascular Research*, **66**(1), 9–11.
- Vanberg, P., & Atar, D. (2010). Androgenic anabolic steroid abuse and the cardiovascular system. *Handbook of Experimental Pharmacology* (195), 411–457.
- Vicencio, J. M., Estrada, M., Galvis, D., Bravo, R., Contreras, A. E., Rotter, D., Szabadkai, G., Hill, J. A., Rothermel, B. A., Jaimovich, E., & Lavandero, S. (2011). Anabolic androgenic steroids and intracellular calcium signaling: A mini review on mechanisms and physiological implications. *Mini - Reviews in Medicinal Chemistry*, **11**(5), 390–398.

- Wagner, S., Dybkova, N., Rasenack, E. C., Jacobshagen, C., Fabritz, L., Kirchhof, P., Maier, S. K., Zhang, T., Hasenfuss, G., Brown, J. H., Bers, D. M., & Maier, L. S. (2006). Ca^{2+} /calmodulin-dependent protein kinase II regulates cardiac Na^+ channels. *Journal of Clinical Investigation*, **116**(12), 3127–3138.
- Wang, J., Li, Z., Du, J., Li, J., Zhang, Y., Liu, J., & Hou, Y. (2019). The expression profile analysis of atrial mRNA in rats with atrial fibrillation: The role of IGF1 in atrial fibrosis. *BMC Cardiovascular Disorders [Electronic Resource]*, **19**(1), 40.
- Weeks, K. L., Bernardo, B. C., Ooi, J. Y. Y., Patterson, N. L., & McMullen, J. R. (2017). The IGF1-PI3K-Akt signaling pathway in mediating exercise-induced cardiac hypertrophy and protection. *Advances in Experimental Medicine and Biology*, **1000**, 187–210.
- Weinsaft, J. W., Kochav, J. D., Kim, J., Gurevich, S., Volo, S. C., Afroz, A., Petashnick, M., Kim, A., Devereux, R. B., & Okin, P. M. (2014). P wave area for quantitative electrocardiographic assessment of left atrial remodeling. *PLoS ONE*, **9**(6), e99178.
- Wilde, A. A. M., Semsarian, C., Marquez, M. F., Sepehri Shamloo, A., Ackerman, M. J., Ashley, E. A., Sternick, E. B., Barajas-Martinez, H., Behr, E. R., Bezzina, C. R., Breckpot, J., Charron, P., Chockalingam, P., Crotti, L., Gollob, M. H., Lubitz, S., Makita, N., Ohno, S., Ortiz-Genga, M., ... Deneke, T. (2022). European Heart Rhythm Association (EHRA)/Heart Rhythm Society (HRS)/Asia Pacific Heart Rhythm Society (APHRS)/Latin American Heart Rhythm Society (LAHRS) Expert Consensus Statement on the State of Genetic Testing for Cardiac Diseases. *Heart Rhythm*, **19**(7), e1–e60.
- Winters, J., von Braunmuhl, M. E., Zeemering, S., Gilbers, M., Brink, T. T., Scaf, B., Guasch, E., Mont, L., Batlle, M., Sinner, M., Hatem, S., Mansour, M. K., Fabritz, L., Sommerfeld, L. C., Kirchhof, P., Isaacs, A., Stoll, M., Schotten, U., & Verheule, S. (2020). JavaCyte, a novel open-source tool for automated quantification of key hallmarks of cardiac structural remodeling. *Scientific Reports*, **10**(1), 20074.
- Wu, L., Bao, J., Liang, E., Fan, S., Zheng, L., Du, Z., Chen, G., Ding, L., Zhang, S., & Yao, Y. (2018). Atrial involvement in arrhythmogenic right ventricular cardiomyopathy patients referred for ventricular arrhythmias ablation. *Journal of Cardiovascular Electrophysiology*, **29**(10), 1388–1395.
- Wu, L., Guo, J., Zheng, L., Chen, G., Ding, L., Qiao, Y., Sun, W., Yao, Y., & Zhang, S. (2016). Atrial remodeling and atrial tachyarrhythmias in arrhythmogenic right ventricular cardiomyopathy. *The American Journal of Cardiology*, **118**(5), 750–753.
- Wu, Y., Zhao, W., Zhao, J., Pan, J., Wu, Q., Zhang, Y., Bauman, W. A., & Cardozo, C. P. (2007). Identification of androgen response elements in the insulin-like growth factor I upstream promoter. *Endocrinology*, **148**(6), 2984–2993.
- Yu, T. Y., Syeda, F., Holmes, A. P., Osborne, B., Dehghani, H., Brain, K. L., Kirchhof, P., & Fabritz, L. (2014). An automated system using spatial oversampling for optical mapping in murine atria. Development and validation with monophasic and transmembrane action potentials. *Progress in Biophysics and Molecular Biology*, **115**(2–3), 340–348.
- Zerbino, D. R., Achuthan, P., Akanni, W., Amode, M. R., Barrell, D., Bhai, J., Billis, K., Cummins, C., Gall, A., Giron, C. G., Gil, L., Gordon, L., Haggerty, L., Haskell, E., Hourlier, T., Izuogu, O. G., Janacek, S. H., Juettemann, T., To, J. K., ... Flicek, P. (2018). Ensembl 2018. *Nucleic Acids Research*, **46**(D1), D754–D761.

Additional information

Data availability statement

The data that support the findings of this study are available from the corresponding author, L.Fa., upon reasonable request.

Competing interests

The authors have declared no direct conflict of interest with regard to the manuscript. L.Fa. has received institutional research grants from governmental and charity funding agencies and several biomedical companies. P.K. has received research support from several drug and device companies active in atrial fibrillation and has received honoraria from several such companies in the past. L.Fa. and P.K. are listed as inventors on two patents held by University of Birmingham (Atrial Fibrillation Therapy WO 01 514 0571, Markers for Atrial Fibrillation WO 2 016 012 783).

Author contributions

L.C.S. performed murine *in vivo* experiments, dSTORM experiments and analysis, gravimetry and histology analysis, RNAseq analysis, P wave analysis in human ECGs and wrote the manuscript. A.P.H. performed and analysed microelectrode, optical mapping, patch-clamp and dSTORM studies, performed gravimetry analysis and wrote the manuscript. T.Y.Y. and C.O.S. set up and performed and analysed optical mapping experiments. D.M.K. designed dSTORM experiments and trained L.C.S. and A.P.H. J.M.P. generated cluster analysis workflows. T.W. and P.M.M. performed histology. F.S. co-designed experiments and trained T.W., T.Y.Y. and S.N.K. A.A. and T.K. screened clinical records according to Task Force Criteria. L.C.S., T.K. and C.O.S. performed semi-automated patient ECG analysis. C.H. prepared RNA samples and co-supervised P.M.M. V.R.C. and G.V.G. analysed RNAseq. M.S. and A.W. performed and analysed RNAseq. S.N.K. and S.B.S. performed *in vivo* experiments and gravimetry. M.O.R. co-supervised T.K. L.Fo. analysed *in vivo* experiments. S.L. trained L.C.S. and co-supervised P.R.M. A.K. performed mass spectrometry of serum DHT concentrations. W.A. and G.G.L. advised on AAS experimental design. D.P. co-supervised C.O.S. R.S. co-supervised A.A. K.G. co-supervised L.C.S. P.K. provided input throughout and co-supervised A.P.H., F.S., C.H. and V.R.C. L.Fa. (co-)supervised L.C.S. A.P.H., T.Y.Y., C.O.S., T.W., F.S., A.A., T.K., V.R.C., S.N.K., C.H., P.R.M., S.B.S., M.O.R. and L.Fo., designed and coordinated the study and wrote

the manuscript. All authors reviewed the results, revised the manuscript and approved the final version.

Funding

This work was partially supported by European Union's Horizon 2020 research and innovation programme (grant agreement no. 633196 [CATCH ME] to P.K. and L.Fa.; no. 965286 [MAESTRIA] to L.Fa.), European Union BigData@Heart (grant agreement EU IMI 116074), British Heart Foundation (FS/13/43/30324 to P.K. and L.Fa.; PG/17/30/32961 to P.K. and A.P.H., PG/20/22/35 093 to P.K.; FS/12/40/29712 to K.G.), German Centre for Cardiovascular Research supported by the German Ministry of Education and Research (DZHK to P.K. and L.Fa.); Leducq Foundation to P.K.; UOB research development fund to L.Fa., T.Y.Y. and C.O.S. studentships were supported by EPSRC to L.Fa. Funding from the Wellcome Trust was received by K.G. (201543/B/16/Z), W.A. (WT209492/Z/17/Z) and C.O.S. (221650/Z/20/Z). K.G. is also funded by the MRC (MR/V009540/1). The Institute of Cardiovascular Sciences is a recipient of a BHF Accelerator Award (AA/18/2/34218). G.V.G. acknowledges support from the NIHR Birmingham ECMC, NIHR Birmingham SRMRC, Nanocommons H2020-EU (731032) and the MRC Health Data Research UK (HDRUK/CFC/01), an initiative funded by UK Research and Innovation, Department of Health and Social Care (England) and the devolved administrations, and leading medical research charities. G.V.G., L.Fa. and W.A. receive support from the NIHR Birmingham Biomedical Research Centre. The views expressed in this publication are those of the authors and not necessarily those of the NHS, the National

Institute for Health and Care Research, the Medical Research Council or the Department of Health.

Acknowledgements

We thank Clara Apicella, Olivia Grech, Pushpa Patel, Genna Riley, Vaishnavi Ameya Murukutla, Hartwig Wieboldt and staff of BMSU Birmingham for expert support. We thankfully acknowledge the Centre of Membrane Proteins and Receptors COMPARE (www.birmingham-nottingham.ac.uk/compare) for both their expertise and infrastructure. We thank the Core Facility Genomics of the Medical Faculty Münster, University of Münster. We thank all members of the Translational Research in Heart Failure and Arrhythmias Cluster in Birmingham and Hamburg for discussion.

Open access funding enabled and organized by Projekt DEAL.

Keywords

arrhythmogenic right ventricular cardiomyopathy, cardiac atria, conduction velocity, desmosome, $\text{Na}_v1.5$, testosterone

Supporting information

Additional supporting information can be found online in the Supporting Information section at the end of the HTML view of the article. Supporting information files available:

Peer Review History

Translational perspective

Our results show that atrial arrhythmias are an important clinical feature of arrhythmogenic right ventricular cardiomyopathy (ARVC) and confirm that males are more likely to show a full ARVC phenotype. We demonstrate a previously unknown interaction between defective desmosomal gene expression and exposure to androgenic anabolic steroids (AAS) in atria. This might explain, in part, the occurrence of atrial conduction slowing and arrhythmias (Akcakoyun et al., 2014; Furlanello et al., 2007; Nieschlag & Vorona, 2015) in athletes using AAS to enhance their performance. Based on our results, searching for desmosomal gene defects in known steroid users with atrial arrhythmias seems warranted. Such analyses might add to a better understanding of the cardiac damage observed in some of these patients.

Our data, gained from well-controlled murine experiments, demonstrate that reduced expression of plakoglobin, as commonly observed in cardiac tissue of patients with pathogenic mutations in a variety of desmosomal genes (Asimaki et al., 2009), renders atria more susceptible to AAS-induced pathology. Prevention of atrial arrhythmias in arrhythmogenic cardiomyopathies is also of interest because they can give rise to inappropriate defibrillator shocks in affected patients (Camm et al., 2013; Takehara et al., 2004) and further compromise heart function.

We add exposure to AAS to the list of stimuli aggravating pro-arrhythmic phenotypes in carriers of desmosomal mutations and demonstrate that this affects atrial electrical function. Our data provide an explanation for the stronger phenotypic expression in male gene carriers with desmosomal mutations and the observed worse clinical outcome in ARVC patients with high physiological testosterone levels (Akdis et al., 2017; Antoniades et al., 2006; Asimaki et al., 2007; McKoy et al., 2000; Protonotarios et al., 2001).